Response to Anonymous Referee #1(Jan07)

This manuscript presents the interesting modeling results on haze in China, and it could be published in the ACPD only with improving English usage.

Response：

The English is improved by a native English-speaker expert and the supplement is their certificate.

Response to Anonymous Referee #3

1) The first sentence of Abstract "The urbanized region of Beijing–Tianjin–Hebei –often shortened to Jing–Jin–Ji and referred to as the 3JNS region in this paper – and its near surrounding region is becoming China's most polluted area by haze, exceeding even the Yangtze and Pearl river deltas." is unnecessary. Please shorten the abstract.

Response:

This is revised in the abstract.

2) In section 2. Model description; please add a brief description about PBL scheme used in the model, because the study presents the PBL modeling results and their analysis.

Response:

A brief description about PBL scheme was in section 4.2 in the manuscript. We move part in section 2 and a brief introduction is also added in the revised manuscript.

3) Page 31684, line 15: Please change "A control (CTL) experiment" with "a simulation" , because there is only one simulation experiment in this paper.

Response:

This is revised in the manuscript.

4) In section 4.2 please replace "planetary boundary layer" with "PBL" as you defined in the abstract. For example. The new title of section 4.2 could be "4.2 Meteorological features of PBL in the haze episode " (Page 31688, line 20)

Response:

This is revised in the manuscript.

5) The quality of some figures is poor, the colors, number and words are hard to identify. Please improve all the figures.

Response:

All figures are redrawn.

Anonymous Referee #1 (Jan 14)

Received and published: 14 January 2015 , Review comment on "Mesoscale modeling study if the interactions between aerosols and PBL meteorology during a haze episode in China Jing-Jin-Ji and its near surrounding region- Part 1: Aerosol distributions and meteorological features" by H. Wang et al.

General comments：

This manuscript, using chemistry transport model GRAPES_CUACE results to investigate aerosol properties including aerosol optical depth (AOD), single scattering albedo (SSA) and asymmetry

parameter (ASY) and meteorological conditions during a haze episode in Jing-Jin-Ji, the national capital region of China also known as biggest urbanized regions in Northern China. The model results are validated with measurements from ground-based stations and space-born satellites (e.g. MODIS, CARSNET, and AERONET). The model simulations are in good agreement with observations and provide the characterized atmospheric aerosol properties during the haze episode. The analysis shows that PBL processes such as horizontal transport and vertical turbulent diffusion within PBL height play a key role in the formation of haze with high PM2.5 concentrations. The results are interesting and the study is meaningful for understanding the formation of the regional haze in China. However, the manuscript is not written in clear and concise English. Please have the manuscript examined by a native English speaker or ask for editor's help to improve the overall language of the paper. I recommend its publication basically in a revision in accordance with the following comments.

Major comments

1. The major analysis in this study pays much attention to comparison between modeled and observed data. I prefer this study, based on interaction between gas/aerosol chemical and physical processes, to answer the question how the haze episode builds up makes more scientific sense and that may require further work.

Response:

Yes, considerable content in this study pays attention to comparison between modeled and observed data. One reason is that the model evaluation is the scientific basic of the following research discussions. Another reason is that this paper is a companion paper of "Mesoscale modeling study of the interactions between aerosols and PBL meteorology during a haze episode in China Jing-Jin-Ji and its near surrounding region – Part 2: Aerosols' radiative feedback effects". The contents of model evaluations of the two papers are all in this paper. The interaction between gas/aerosol chemical and physical processes is certain important and scientific meaningful for haze episode and we will study it exclusively in the following work.

2. The introduction to datasets used for the model initialization and updating boundary conditions is not clear for both chemistry and meteorology. Line 8 on Page 31685: "The initial values of all tracer gases and aerosol concentrations are based on the 24h forecast made by the previous day's model run". I am wondering what data are used for initialization at very beginning of model runs. Do not you use simulations from global (or over a larger domain) chemical transport model to serve as initialization and time-dependent boundary conditions?

Response:

NCEP 1*1 Reanalysis data were used for the model's initial and 6 h meteorological lateral boundary input fields (please see line 6-8 on page 11)

The monthly climate mean values of all tracers from observation data are used for initialization at the very beginning of model run. The initial values of all tracer gases and aerosol concentrations are based on the 24h forecast made by the previous day's model run during the model runs. The simulation results after the first three days' model runs are used in this study for eliminating the model errors from the chemical tracer initialization.

Minor comments

1. Line 8 on Page 31685: "The initial values of all tracer gases : : :" might be "The initial

values of all long-lived gases in RADM2: : :". As per my under- standing, tracer gases are inert in chemistry.

Response:

Not only "long-lived gases", but also SO2, NO2 and NH3 etc. are included in the gases. It should be "The initial values of all gases in RADM2 "

2. Line 26 in Abstract: "The momentum transmitting downward of the cold air from above the PBL to the low PBL and surface lead to an increase in surface wind speeds and haze dispersal" may be changed into "The cold air above PBL with high momentum downward to lower atmosphere and surface layer is responsible for increase of surface wind speed. That leads to decreasing of PM2.5 concentration".

Response:

This is revised in the manuscript.

3. Line 4 on Page 31679: What is the definition of "pollution strength".

Response:

Pollution strength means PM2.5 values here. " pollution strength ($PM_{2.5}$)" may be better here.

4. Line 5-14 on Page 3167: The presentation in this part is not clear. Please re-write clearly, correctly, and concisely.

Response:

I am sorry that Page 3167 can't be found.

5. Line 2 on Page 31685: ": : :, formed the simulation basis of this research." may be changed to ": : :, serve as the base simulations for this research."

Response:

This is revised in the manuscript.

6. Line 20 on Page 31685: ": : : which fills in data gaps left by : : :" might be ": : : which fills in data gaps remaining in : : :".

Response:

This is revised in the manuscript.

7. Line 22 on Page 31686: ": : : (SACOL) station on the Lanzhou University campus : : :" should be ": : :(SACOL) station located at the Lanzhou University campus : : :".

Response:

This is revised in the manuscript.

8. The first paragraph of section 4.2 need to be re-written because it is not logically clear on PBL and processes involved in PBL.

Response:

This paragraph is re-written in the manuscript according to the reviewer's' opinion and it is moved to section 2 according to another reviewer's' opinion.

Mesoscale modeling study of the interactions between aerosols and PBL meteorology during a haze episode in China Jing-Jin-Ji and its near surrounding region: Part 1. aerosol distributions and meteorological features

H. Wang[1,2*], M. Xue[1*], X. Y. Zhang[1], H. L. Liu[1], C .H. Zhou[1], S. C. Tan[3], H. Z. Che[1]， B. Chen[3], T. Li[4]

1 Institute of Atmospheric Composition(IAC), Key Laboratory of Atmospheric Chemistry (LAC) of China Meteorological Administration (CMA),Chinese Academy of Meteorological Sciences (CAMS), Beijing, 100081, China
2 Collaborative Innovation Center on Forecast and Evaluation of Meteorological Disasters, Nanjing University of Information Science & Technology, Nanjing 210044, China
3 State Key Laboratory of Numerical Modeling for Atmospheric Sciences and Geophysical Fluid Dynamics (LASG), Institute of Atmospheric Physics, Chinese Academy of Sciences, Beijing, 100029, China
4 School of Atmospheric Physics, Nanjing University of Information Science & Technology, Nanjing 210044,China

Corresponding author: wangh@cams.cma.gov.cn; xm@cams.cma.gov.cn

Abstract

The urbanized region of Beijing-Tianjin-Hebei ~~– often shortened to Jing-Jin-Ji and referred to as the 3JNS region in this paper –~~ and its near surrounding region is becoming China's most polluted area by haze, exceeding even the Yangtze and Pearl river deltas. Aside from pollutant emission, the meteorology of the planetary boundary layer (PBL) is the most important factor affecting haze pollution. Focusing on July 2008, the aerosol optical properties and PBL meteorology features closely related with haze formation were simulated in 3JNS region using an online atmospheric chemical transport model. The relationship between regional PBL meteorology, $PM_{2.5}$, and haze is discussed. Model results accurately simulated the aerosol optical depth (AOD), single scattering albedo (SSA) and asymmetry parameter (ASY), validate by comparison with observations from the MODerate Resolution Imaging Spectroradiometer (MODIS), the China Aerosol Remote Sensing NETwork (CARSNET) and the Aerosol Robotic NETwork (AERONET). Modeled PBL wind speeds showed reasonable agreement with those from the National Centers for Environmental Prediction (NCEP) Reanalysis 2. A monthly mean AOD value as high as 1.2 was found from both model and observations, with a daily mean larger than 2.0 during haze episodes in the 3JNS Region. Modeled and observed SSA values of 0.90–0.96 and ASY values of 0.72–0.74 demonstrated the high scattering characteristic of summer aerosols in this region. PBL wind speeds from modeled and NCEP data both showed a reversing trend of $PM_{2.5}$ variation, illustrating the importance of the "PBL window shadow" on haze formation. Turbulence diffusion and PBL height showed had opposite phases to surface $PM_{2.5}$, indicating that lower PBL height and weaker PBL turbulence diffusion are essential to haze formation. It is noted that homogeneous air pressure does not occur at the surface but at an 850–950 hPa height during the haze episode.

49 The momentum transmitting downward of the cold air from above the PBL to
50 the low PBL and surface lead to an increase in surface wind speeds and haze
51 dispersal.

52

1. Introduction

With its rapidly expanding urbanization, and both economic and industrial developments, China is faced with increasing poor air quality and haze pollution. There are three main haze pollution regions in eastern China: the Yangtze River delta, the Pearl River (Zhu Jiang) delta, and Beijing-Tianjin-Hebei (shortened to Jing-Jin-Ji) and its near surroundings region (3JNS). These are all areas of high population, rapid economic growth, urbanization and energy consumption *(Zhang et al., 2004; Chak et al., 2008; Che et al., 2009; Wu et al., 2010)*. The Yangtze River Delta region consists of Shanghai, the urban agglomeration of southeast Jiangsu Province and northeast Zhejiang Province. The Pearl River delta metropolitan area includes Guangzhou, Shenzhen, Dongguan, Zhuhai and other nearby cities. The 3JNS Region includes Beijing (Jing), Tianjin (Jin) and Hebei Province (Ji) and their near surroundings including eastern Shanxi province, western Shandong province and northern Henan province.

Many observational and modelling studies have focused on pollution in the Yangtze River delta *(Zhang et al., 2008; Fu et al., 2008; Yin et al., 2009; Gao et al., 2009; Gao et al., 2011; Wang et al., 2012; Kang et al., 2013)* and Pearl River delta regions around the time of their initial, rapid economic development *(Zheng et al., 2000; Lee et al., 2001; Cao et al., 2004; Wu et al., 2006; Chan et al., 2006; Chak et al., 2008; Huang et al., 2008; Tan et al., 2009; Tan et al., 2011)*. However, the 3JNS region has recently become the most polluted area of the three regions and is now attracting serious concern *(Wang et al., 2006; Chen et al., 2007; Wu et al., 2008; Wei et al, 2010; Liu et al., 2010; Wang et al., 2012; Duan et al., 2012; Wang et al, 2014a, 2014b; Che et al., 2014)*. According to the China Environmental Condition Report by the Ministry of Environmental Protection of The People's Republic of China (MEPPRC), seven of the top ten polluted cities in China in the first six months of 2013 –

Xingtai, Shijiazhuang, Handan, Baoding, Tangshan, Hengshui and Langfang – are located in this region However, haze pollution and air quality studies in this region, especially modeling and simulation studies, are rare *(Wang et al., 2008; Xing et al., 2011)* and inadequate compared to the Yangtze River delta and Pearl River delta regions *(Westerdahl, et al., 2009; Zhang et al., 2009, 2013; Zhang et al., 2011; Quan, et al., 2014; Wang et al., 2014a).*

When haze occurs, local meteorological patterns strongly affect the transport and mixing of gases and aerosols, pollutant loading, spatiotemporal distributions and pollution strength. In particular, the meteorological conditions of the local planetary boundary layer (PBL), *e.g.* wind fields, turbulence diffusion, PBL height and atmospheric circulation patterns, are all key to hazy weather, and dominate whether the haze occurs or not since emissions can remain stable within a defined period in a certain area. A PBL parameterization scheme and describing local PBL meteorological conditions in mesoscale atmospheric chemistry models form the base of $PM_{2.5}$ and haze forecasting. In turn, high particle concentrations suspended in the PBL atmosphere during hazy weather may exert a remarkable influence on local PBL meteorology and circulation patterns by reforming the regional solar and thermal radiative budgets.

Focusing on July 2008 over the 3JNS Region, this paper outlines the methodology for the online calculation of aerosol optical features of different species based on an external mixing scheme, introduced into the atmospheric chemical model GRAPES-CUACE for simulating the aerosol optical features and PBL meteorology condition. The local aerosol optical, meteorological and circulation pattern in the PBL as related to haze are also discussed, with a particular focus on the haze episode of July 7–11, 2008. The relationship between key PBL meteorological factors, $PM_{2.5}$ and the haze episode is analyzed. The impact of aerosols on local PBL is presented in a companion

paper (Part II).

2. Model Description

The Chinese Unified Atmospheric Chemistry Environment (CUACE) has been integrated into the mesoscale version of Global/Regional Assimilation and PrEdiction System (GRAPES_Meso) developed by the Chinese Academy of Meteorological Sciences, China Meteorological Administration (CMA), to build an online chemical weather forecasting model, GRAPES-CUACE/haze, focusing especially on haze pollution forecasting in China and East Asia. An aerosol radiative parameterization scheme was incorporated into the GRAPES-CUACE model. The aerosol optical depth (AOD), single scattering albedo and asymmetry factor (ASY) is calculated online using this model. The following sections offer a brief introduction to the model.

2.1 GRAPES_Meso

GRAPES_Meso is a real-time operational weather forecasting model used by the CMA, which includes 3-D meteorological field data assimilation, a fully compressible non-hydrostatic model core and a modularized physics package (*Chen et al., 2003; Zhang and Shen, 2008; Chen et al., 2008; Yang et al., 2007*). The model's time integration discretization uses a semi-implicit and semi-Lagrangian temporal advection scheme. The model's horizontal discretization adopts an Arakawa-C staggered grid arrangement and a central finite-difference scheme with second order accuracy, while the model's vertical discretization adopts a non-hydrostatic approximation scheme. Height-based, terrain-following coordinates are used. The model's vertical discretization adopts the vertically-staggered variable arrangement proposed by Charney–Phillips. The large-scale horizontal and vertical transportation and diffusion processes for all gases and aerosols are processed in the dynamic frame of GRAPES_Meso. The GRAPES_Meso3.3 model was released in July

2013 and was used in the GRAPES-CUACE/haze in this study.

The physical processes principally involve large-scale condensation, cumulus convection, micro-physical precipitation, radiative transfer, land surface and boundary layer processes. Each physical process incorporates the use of several schemes *(Xu et al., 2008)*. The model physics schemes and the related lead references used in this study are summarized and list in Table 1. The PBL scheme is very important for correctly modeling and providing accurate weather forecasts (Vogelezang et al., 1996; Santanello et al., 2005), especially for accurate air pollution forecasts (Cheng et al., 2002; Pleim, 2007b). The PBL is the lower tropospheric layer with its height (PBLH) ranging from several hundred meters to a few kilometers, which is one basic feature to the accurate and realistic modeling. The processes of heat, moisture and momentum exchange between the Earth's surface and the rest of the atmosphere all occur within the PBL. The wind speed near the surface, turbulence diffusion, and stability are also calculated in PBL scheme in air quality model. Among the different definitions of PBL, there are still some general agreements. Richardson number (Ri) is usually used by PBLH calculation. A height at which the local Richardson number exceeds a critical value is used to separate stable from turbulent flow. The Hong and Pan Medium Range Forecast (MRF) PBL scheme (Hong and Pan, 1996) was selected for this study (Table 1). The MRF PBL scheme uses nonlocal closure and rely heavily on Ri to compute PBLH. It define PBLH as the height at which a critical Ri is reached 0.5. All the PBL parameters discussed in the following sections are based upon this PBL scheme.

2.2 CUACE

Components of the atmospheric chemistry model CUACE include an emission inventory and process system; gaseous, physical aerosol and chemistry processes; and related thermodynamic equilibrium modules for

processing the transformation between gas and particle matter *(Gong and Zhang, 2008; Wang et al., 2009; 2010)*. The CUACE module tracer consists of 66 gas species and seven species of aerosols, with 12 particle size bins.

2.2.1 Emissions

Based on official information about national emission sources in 2006 *(Cao et al., 2006)*, the detailed high-resolution emission inventories of reactive gases, *i.e.* SO_2, NO_x, CO, NH_3 and VOCs, from emissions over China in 2007 were updated to form the current emission data *(Cao et al., 2010)*. The Sparse Matrix Operator Kernel Emissions system (SMOKE) was used to transform this emission data into hourly gridded data as required by the GRAPES_CUACE model, which includes five aerosols species (black carbon (BC), organic carbon (OC), sulfate, nitrate and fugitive dust particles) and 27 gases including VOCs, NH_3, CO, CO_2, SO_x and NO_x *(An et al., 2013)*.

2.2.2 CUACE/Gas

CUACE/Gas is based on the Regional Acid Deposition Model (RADM) *(Stockwell et al., 1990)*, which consists of 66 gaseous species, including five second-order organic aerosols (SOA); 21 photochemical reactions and 121 gas phase reactions are also involved. Wet and dry deposition processes, simple SOA reactions and a liquid phase chemical balance are also included. The gas to aerosol particle transformation process is described using a thermodynamic equilibrium equation.

2.2.3 CUACE/Aero

There are seven species of aerosol considered in CUACE/Aero: sulfates (SF), soil dust (SD), black carbon (BC), organic carbon (OC), sea salts (SS), nitrates (NI) and ammonium salts (AM). The model divides all the aerosol particles into 12 particle size bins with diameter ranges of 0.01–40.96 μm

(excluding AM). CUACE/Aero includes the major aerosol processes in the atmosphere: hygroscopic growth, coagulation, nucleation, condensation, dry deposition and sedimentation, below-cloud scavenging, aerosol activation, aerosol–cloud interactions and chemical transformation of sulfur species *(Gong and Zhang, 2008)*.

2.3 On-line Calculation of Optical Properties of Externally-mixed Aerosols

Aerosol chemical properties and sizes are used to calculate aerosol optical and radiative properties. Each chemical constituent of an aerosol is associated with a set of complex refractive index (CRI) data as a function of wavelength. The CRI data of the seven species of aerosols are derived mainly from the HITRAN 2008 database *(Rothman et al., 2009)*, and the Optical Properties of Aerosols and Clouds database (OPAC) *(Hess et al, 1998)*. Optical model data, accounting for East Asian dust using both theory calculation and composition analysis of aerosol samples collected in the Chinese desert during the international project, “Studies on the Origin and Transport of Aeolian Dust and its Effects on Climate” (ADEC), is used to account for Chinese mineral dust CRI data *(Wang et al., 2004; 2006)*. Based on these CRI data and particle sizes in GRAPES_CUACE, Mie theory is used to calculate the key optical parameters of dry aerosol particles in determining aerosols’ direct radiative effects, *i.e.* the extinction coefficient (Q_e), the SSA and the ASY. The mass extinction coefficient (K_{ext} in $m^2\ g^{-1}$) is calculated according to the following formula:

$$Kext_{m,n}(\lambda) = 3Qe_{m,n}(\lambda)/4r_n\rho_m \quad (1)$$

where n represents the particle bin from size 1 to 12 and r_n is the corresponding effective radius of the n^{th} aerosol size, ρ is the particle mass density of the particular aerosol calculated, and m is the aerosol species, *i.e.*

BC, SF, SD, BC, OC, SS, NI or AM, and λ is the wavelength. Figure 1 shows the K_{ext} (Fig. 1a), SSA (Fig. 1b) and ASY (Fig. 1c) for six radii of the model's 12 dry particle size bins (R_dry) from small to large particles of seven species of aerosol. The red line in Fig. 1 indicates the representative particle size bin for the species of aerosol with the highest concentration in the model. For SD aerosol particles, the size range is relatively large and all particle size bins are used, while for AM aerosol particles, only the particle size bin with a radius of 0.06μm is employed. It can be seen from Fig. 1 that the optical features of dry aerosol particles change with chemical composition, particle size and wavelength. These changes are described in the following study of the aerosol radiative parameterization scheme. The AOD of any of the 12 particle bin sizes for any seven of the aerosol species is calculated using:

$$AOD_{m,n}(\lambda) = \sum_{i=1}^{k} Kext_{m,n}(\lambda) C_{m,n} \Delta z_i \quad (2)$$

where $C_{m,n}$ is the mass concentration of the aerosol, n stands for the n^{th} particle size bin and m indicates the aerosol type, i is the index of vertical layers, K is the total number of layers in the model, and Δz_i is the thickness of the model layer. For hygroscopic aerosols, *i.e.* SF, OC, SS, NI and AM, aerosol sizes of wet particles are calculated as a function of relative humidity (RH) using the Kola equation. A total of 10 RH values, 0%, 45%, 50%, 60%, 70%, 80%, 90%, 95%, 98%, and 99%, are considered in the model. The AOD, SSA and ASY of wet particles are a function of chemical composition, RH, particle size and wavelength, which are described as $AOD_{m,n}(rh, \lambda)$, $SSA_{m,n}(rh, \lambda)$ and $ASY_{m,n}(rh, \lambda)$. Figure 2 shows the typical particle size of the above three optical factors (the red line in Fig.1) for five hygroscopic aerosol species at six different RHs. It can be seen from Fig. 2a that the extinction efficiencies of different aerosol species, and their changing trends along with

wavelength and RH, are distinctly diverse. Wet aerosols SSA (Fig. 2b) and ASY (Fig. 2c) also show similar dependencies on RH, particle size and chemical composition. Figure 2 indicates a detailed aerosol radiation parameterization scheme considering particle size, atmospheric RH and the particle chemical aerosol composition is essential to evaluate aerosol radiative feedback. An external mixing scheme is used for the different particle size bins for one aerosol type and for different aerosol species to calculate composite aerosol optical properties for each model grid, according the following formulae:

$$AOD\ （rh,\lambda）=\sum_{m=1}^{7}\sum_{n=1}^{12}AOD_{m,n}（rh,\lambda）\tag{3}$$

$$\mathrm{SSA}(rh,\lambda)=\frac{\sum_{m=1}^{7}\sum_{n=1}^{12}SSA_{m,n}(rh,\lambda)\times AOD(rh,\lambda)_{m,n}}{AOD(rh,\lambda)}\tag{4}$$

$$ASY(rh,\lambda)=\frac{\sum_{m=1}^{7}\sum_{n=1}^{12}AOD_{m,n}(rh,\lambda)\times SSA_{m,n}(rh,\lambda)\times ASY_{m,n}(rh,\lambda)}{\sum_{m=1}^{7}\sum_{n=1}^{12}SSA_{m,n}(rh,\lambda)\times AOD(rh,\lambda)}\tag{5}$$

Composite aerosol optical properties change with particle size bin (n) and concentration (C_m); RH forecast according to the GRAPES_CUACE model; and wavelength (λ) according to formulae 1–5.

3. Experiment Design

A ~~control (CTL)~~simulation experiment was achieved in this study through treating any composite aerosol only as a dynamic tracer: the aerosol's radiation feedback to its dynamic process was not calculated in this model experiment.

The model run for this study commenced on June 25, 2008 and the simulated results for July 1–31, 2008, serve as the base simulations for this researchformed the simulation basis of this research. The GRAPES_CAUCE3.0 model adopts an alterable horizontal resolution, a time step and a forecasting time. There are 31 model layers ascending vertically from the Earth's surface to 31km height. For the purposes of this study, the horizontal resolution was set to 0.15°×0.15°, the time step to 100 s and the forecasting time to 72 h. The model domain was set as 90–140°E, 20–55°N. NCEP 1×1° Reanalysis data were used for the model's initial and 6 h meteorological lateral boundary input fields. The monthly mean values of all tracers from observation data are used for initialization at the very beginning of model run. The initial values of all tracer gases in RADM2 and aerosol concentrations are based on the 24 h forecast made by the previous day's model run. The simulation results after the first three days' model runs are used in this study for eliminating the model errors from the chemical tracer initialization.

4. Results

4.1 Optical properties of aerosols

AOD is a good parameter for elucidating aerosol column loading in the atmosphere. Aerosol optical properties contributing to AOD, SSA and ASY are the most direct and critical parameters for aerosol direct radiative forcing, radiative heating effects, and feedback to atmospheric circulation (*Wang et al., 2006; Huang et al., 2006, 2009*). AOD data from the Moderate Resolution Imaging Spectroradiometer (MODIS), onboard the Aqua satellite, have been widely used in evaluating and investigating the aerosol burden (*Ichoku et al., 2002; Kahn et al., 2007; Zhang and Reid, 2010*). The daily MODIS AOD by Deep Blue algorithm, which fills in data gaps remaining inwhich fills in data gaps left by the Dark Target-Land aerosol retrieval over bright surfaces (*Hsu et*

al., 2006), at 550 nm (MODIS/Aqua Collection 5.1 MYD08_D3 product) with a spatial resolution of 1°×1° is used in this paper to evaluate the modeled AOD.

Figure 3 compares the modeled monthly averaged AOD for July with MODIS Deep Blue AOD at 550 nm. It can be seen from Fig. 3 that both the MODIS and modeled AOD results show that the highest AOD values are in the 3JNS region, reaching 1 for most of this region and even 2. As a general rule, the modeled AOD results seem a little higher than the MODIS AOD data. Considering the uncertainties of MODIS Deep Blue AOD over land (*Remer et al., 2005*), especially in spring and summer time in eastern China (*Yang et al., 2011*), its time-limited scans of China, and the different integrating time of the monthly averaged MODIS and modeled AOD, the resulting consistency of the horizontal distribution, the AOD's central location, and the values of both AOD data sets is both acceptable and reasonable. These results also prove the model's performance in July 2008 in describing aerosol column loading and the extinction effects by the composite atmospheric aerosol in this region.

The ground based observed AOD from the China Aerosol Remote Sensing NETwork (CARSNET) (*Che et al., 2008*) is also employed to evaluate the modeled AOD. CARSNET AODs are retrieved in the 440, 675, 870, and 1020 nm bands using the automatic Cimel sun and sky scanning radiometer (Cimel-318, Cimel Electronique). Taking the data continuity and the locations of the stations into account, the AOD at 440 nm at six surface CRASNET stations are used here. The locations and altitudes of these stations are listed in Table 2. The Beijing, Xianghe and Shangdianzi stations are all located in the Beijing metropolitan region. The Beijing station is located in CMA premises, and was taken as representative of urban Beijing, while the Xianghe and Shangdianzi stations are located in the rural areas around Beijing. The city of Lanzhou is taken as having air pollution conditions typical of western China. The Lanzhou CARSNET station is located in urban Lanzhou; the Semi-Arid

Climate and Environment Observatory of Lanzhou University (SACOL) station located in the Lanzhou University campus~~on the Lanzhou University campus~~ in Yuzhong, outside the city, represents the rural region of Lanzhou (Huang et al., 2008). The Gucheng station located in Hebei Province represents Beijing's periphery. Datong is a medium-sized city in Shanxi Province, westward and windward of Beijing. All the stations are located in mideastern China, except for Lanzhou.

Figure 4 shows a comparison between daily averaged CRASNET and modeled AOD data in July, 2008. It can be seen that both the simulated and the observed AOD data congruously indicate two pollution episodes in the 3JNS Region, one from 7 to11 July, 2008, in Beijing, Shangdianzi, Gucheng and Datong, and another from 23 to 29 July, 2008 in Beijing, Shangdianzi and Gucheng. Both modeled and observed AOD data show that the daily averaged AOD values reached 1.5–3 during the episode on 7–11 July, 2008, indicating that the pollution affects not only Beijing and its environs, but also Shanxi Province (i.e. Datong) to the west. The 23–29 July, 2008 pollution episode appears weaker, but lasted longer than the episode on 7–11 July, 2008, and was not observed at the Datong station. The modeled and CARSNET AOD data from 1–31 July, 2008 shows fairly consistent diurnal trends, validating the modeled AOD data at these four stations. In Lanzhou, CARSNET AOD values remained low from 1 to 31 July, 2008, and almost all were <0.5, indicating clear air conditions in this city in July. Modeled AOD values show very similar results with the observed CARSNET data, corroborating the model's validity for western China. For Longfengshan station in northeastern China, the model's performance is not as good as for other stations as compared to CARSNET AOD data.

SSA and ASY values also have a substantial impact on aerosol radiative effects and feedback to atmospheric circulation, which help determine the

existence of aerosol radiative forcing, *i.e.* the heating or cooling of the atmosphere, and the negative or positive radiative feedback from the haze episode itself. The SSA and ASY observation data set from the Aerosol Robotic Network (AERONET) at the Xianghe and SOCAL stations were used to evaluate the model's performance. Monthly averaged AERONET and modeled SSA and ASY were calculated, together with the SSA and ASY bias for the model (Table 3). It can be seen from Table 3 that observed SSA at the Xianghe station was 0.96, and 0.95 at the SOCAL station; the modeled values were 0.93 and 0.90 for the two stations, respectively. AERONET and modeled SSA data for the two stations consistently indicate a high aerosol scattering ratio in western and eastern China. The SSA bias is −3% at the Xianghe station and −5% at the SOCAL station. The AERONET ASY is 0.74 at the Xianghe station and 0.72 at the SOCAL station, while the modeled values are 0.78 and 0.77, respectively. The ASY bias is +5% at the Xianghe station and +7% at the SOCAL station. The SSA and ASY bias for the model is therefore both reasonable and acceptable, taking the experimental sensitivity of the impact of optical properties on radiative forcing into account *(Wang et al., 2006)*. It is worth noting that both the SSA and ASY observed data sets for the Chinese mainland are sparse. Only 10 days' SSA and ASY data for the Xianghe station, and seven days' SSA data and 17 days' ASY data for the SOCAL station were available for evaluating this study's modeled results.

The vertical distribution of the aerosol layer is the other key factor affecting aerosol radiation besides chemical composition and optical characteristics. Diurnal changes in the vertical distribution of $PM_{2.5}$ for the 3JNS region from 1–31 July, 2008 were calculated and are displayed in Fig. 5a. It can be seen that the $PM_{2.5}$ pollutants were generally concentrated in the surface and near surface atmosphere in July, 2008. A $PM_{2.5}$ concentration >120 μg m^{-3} generally occurs below 800 hPa, overlapping the PBL height, or a little higher. The greatest height of the concentrated $PM_{2.5}$

layer varies between 700 hPa to 900 hPa on different days. Figure 5b shows the vertical distribution of averaged $PM_{2.5}$ and K_{ext} for 7–11 July, 2008. A $PM_{2.5}$ concentration >150 μg m^{-3} occurs below 900 hPa and a concentration of >110 μg m^{-3} is found below 800 hPa. The highest K_{ext} value appears at 800 hPa, suggesting that the greatest aerosol extinction occurs in the upper PBL, or above it, aiding the cooling of the lower PBL and the heating of the upper PBL.

4.2 P~~lanetary boundary layer~~BL meteorological features corresponding to the haze episode

~~The PBL is the lower tropospheric layer and has a height ranging from several hundred meters to a few kilometers. The PBL is very important for correctly modeling and providing accurate weather forecasts *(Vogelezang et al., 1996; Santanello et al., 2005)*, especially accurate air pollution forecasts *(Cheng et al., 2002; Pleim, 2007b)*. The wind speed near the surface, the turbulence diffusion process and stability are all calculated in the PBL. The processes of heat, moisture and momentum exchange between the Earth's surface and the rest of the atmosphere also occur within the PBL.~~

The PBL wind speed, diffusion coefficient and PBL height are the most important parameters representing the PBL characteristics affecting air and haze pollution. The terms "window shadow", "homogeneous air pressure" and "stable and steady" have been used to describe the typical patterns of local air circulation and surface meteorological fields for haze episodes. In the following section, these three factors and their correlation with particulate $PM_{2.5}$ pollutants are discussed. Air pressure patterns are also used to discuss the strength of, and changes in, PBL cold air; these patterns have an important effect on air pollution episodes, and most especially upon the weakening and collapsing of haze episodes.~~ The Hong and Pan Medium Range Forecast PBL scheme *(Hong and Pan 1996)* was selected for use in the GRAPES_CUACE model; all the PBL parameters discussed in the following sections are based~~

~~upon this scheme.~~

4.2.1 Planetary boundary layer winds

Not only do the surface winds directly impact haze impacts, but also the winds in the whole PBL. The accuracy of the model's forecasting of surface and PBL winds is critical for an accurate haze prediction. The conventional meteorology observation data from sounding balloons are only available at 00:00 and 12:00 UTC in China (early morning or dust in local time). The NCEP/NCAR Reanalysis-2 meteorology data are available for numerous meteorological parameters including geopotential height, air temperature, vertical velocity, wind field, etc., at a time resolution of 6 hours (00:00, 06:00, 12:00, and 18:00 UTC) at sea level pressure, 1000, 950, 850, 700, 500, 300 hPa, etc. heights. In view of the importance of daytime PBL meteorology conditions to haze episode, Reanalysis-2 data are used to evaluate the model's results and study the PBL features instead of sounding balloon observations, due to the lack of daytime PBL meteorology data from the latter.

Figure 6 shows the model's daily averaged wind speeds and the NCEP analysis for the 3JNS Region for 1–31 July, 2008, together with $PM_{2.5}$ at the surface (Fig. 6a) and at 850–950 hPa (Fig. 6b). It can be seen that the modeled wind speed at 850–950 hPa agrees well with the NCEP wind speed, showing the model's fair ability to predict wind speed at this height. Averaged modeled $PM_{2.5}$ for the same region at 850–950 hPa is also shown in Fig. 6a. It can be seen that the diurnal variations in $PM_{2.5}$ in the PBL evince a completely contrary phase, shifting with the wind speeds of both modeled and NCEP Reanalysis, *i.e.* the peak values of $PM_{2.5}$ correspond with the trough values of wind speed, showing that low wind speed in the PBL may be the most important factor leading to haze pollution. Modeled surface wind values also correspond fundamentally with NCEP data, though not at 850–950 hPa. Nonetheless, the modeled surface wind speed and $PM_{2.5}$ show opposing trends, similar with the 850–950 hPa findings. Corresponding wind speeds are

as low as 0.5 m s^{-1} at the surface and are <2m s^{-1}, rising to 4–5m s^{-1} at 850–950 hPa separately during the severe haze pollution episodes of 7–11 and 25–28 July, 2008.

4.2.2 Planetary boundary layer turbulence diffusion

Turbulence diffusion is another important process significantly affecting surface pollutant concentration, since it defines horizontal transportation distance by affecting the vertical heights that pollutants may reach. The turbulence diffusion coefficient (*fktm*) parameterizes the PBL turbulence diffusion process *(Wang et al., 2010)*. Figure 7 shows the averaged surface $PM_{2.5}$ and f_{ktm} horizontal distribution for 7–11 July, 2008 (Fig. 7a), together with the diurnal changes of the 3JNS averaged $PM_{2.5}$ and f_{ktm} (Fig. 7b) from 1 to 31 July, 2008. Figure 7a shows that lower f_{ktm} and higher $PM_{2.5}$ values occurred throughout mid- and eastern China during 7–11 July, 2008. The lowest f_{ktm} values and highest 400 $PM_{2.5}$ values appeared in the 3JNS region, showing the importance of turbulence diffusion on the strength of severe air pollution. It also can be seen from Fig. 7a that $PM_{2.5}$ concentrations exhibit higher values when f_{ktm} are lower, and that this is more marked over the 3JNS region than over southeastern China (22–30°N, 110–120°E). The daily averaged f_{ktm} and $PM_{2.5}$ values for the 3JNS region (Fig. 7b) show a marked correlation over the severely polluted parts of this region. There is a basic reverse trend in daily f_{ktm} and $PM_{2.5}$ values.

4.2.3 Planetary boundary layer height

PBL height is one of the most important variables in any PBL scheme. PBL height can be variously defined by reference to the local Richardson number, the height of the capping inversion, the proportionality of PBL height to the ratio between the friction velocity and the local Coriolis force parameter, the height of the minimum sensible heat flux, turbulent kinetic energy, or a

specific vertical potential temperature gradient *(Cheng et al., 2002; Santanello, et al., 2005; Hong et al., 2006; Pleim et al., 2007b)*. Despite all these different definitions, some commonality of agreement on the definition of PBL height exists, *e.g.* the Richardson number, the capping inversion or the height where the potential temperature lapse rate becomes too positive, and so on. The medium-range forecast (MRF) PBL scheme uses non-local closure and relies heavily on Richard index (*Ri*) to compute the PBL height for different regimes (*Hong and Pan, 1996*).

Figure 8 shows the horizontal distribution of the averaged surface $PM_{2.5}$ and PBL height for 7–11 July, 2008 (Fig. 8a), together with diurnal regional trends in the 3JNS averaged $PM_{2.5}$ and PBL height (Fig. 8b). The PBL height values (Fig. 8a) are as low as 300–900 m with high $PM_{2.5}$ values over eastern China, consistent with observational studies of this region *(Wang et al., 2012)*. The lowest PBL height almost overlaps with the regions of lowest f_{ktm} and highest $PM_{2.5}$ over mideastern China for this period. Comparing the similarly economically developed areas of mideastern and southeastern China (22–30°N, 110–120°E), mideastern China is much more severely polluted. This would suggest that a lower PBL height and weak turbulence diffusion (Fig. 7a) may be two of the main factors leading to higher pollution over this area. Diurnal changes in averaged PBL height and $PM_{2.5}$ over the central polluted area (Fig. 8b) also display a generally contrary correlation during July 2008, indicating the important impact of the PBL height on the pollution strength (PM2.5 concentration) of the surface air, *i.e.* low PBL height and f_{ktm} are critical to the degree of haze pollution.

4.2.4 Patterns in planetary boundary layer air pressure fields

Surface “homogeneous air pressure” has been regarded as a typical surface air pressure feature associated with haze pollution *(Liu et al., 2010)*. Detailed comparisons of PBL air pressure patterns between hazy and clear

conditions for different seasons are, at present, limited. Modeled $PM_{2.5}$, AOD and CARSNET AOD data (Fig. 4) all show that July 10, 2008, was the severest haze day, while July 12, 2008, was the first clear day after this haze episode. Figure 9 displays the air pressure pattern, wind speed vector at the surface (bottom), geopotential height and wind speed vector at 950 hPa (middle) and 850 hPa (top) on 10 July, 2008 (left), and 12 July, 2008 (right). July is midsummer in China and a subtropical high with high pressure contolled the surface in eastern China and the sea region east of China on 10 July, 2008. No obvious difference was observed between the surface air pressure pattern on 12 July, 2008 and on 10 July, 2008 due to the effect of the strong subtropical high to the east. The patterns of geopotential heights for 850–950 hPa heights are quite different from those for surface pressure, showing a “homogeneous air pressure pattern” over the whole of eastern China on 10 July, 2008. The southeasterly weakening and retrenchment of the subtropical high from 10 to 12 July, 2008 is clear at 850–950 hPa height. The main area of subtropical high pressure withdrew across the sea west of the Korean Peninsula on 12, 2008. At the same time, cold air from Mongolia moved to midnorthern China, and the air pressure over this region strengthened at 850–950 hPa during 10–12 July, 2008. Eastern China was controlled by continental high pressure from the northwest, increasing the northerly wind speed over mideastern China at 850–950 hPa on 12 July, 2008. The surface wind vector shows that over mideastern China, the northerly wind speed on 12 July, 2008, was obviously higher than that on 10 July, 2008. This was not caused by any pressure-gradient force because the air pressure patterns on 10 and 12 July, 2008, were very similar, but the transfer of cold air and momentum from 850–950 hPa to the surface led to an increase in the northerly wind speed at the surface, directly bringing the haze episode to an end over the mid- and eastern China including the 3JNS Region.

5. Conclusion

518 The mesoscale chemical weather forecasting model
519 GRAPES-CUACE/haze, integrated with an online radiative parameterization
520 scheme, based on an external mixing scheme of black carbon, organic carbon,
521 soil dust, nitrates, sulfate, sea salt and ammonia aerosols, was employed to
522 simulate the optical characteristics of aerosols and the PBL meteorological
523 features related to haze in July 2008. The aerosols' AOD, SSA and ASY
524 features were simulated and evaluated. The PBL characteristics of aerosol
525 loading, PBL heights, turbulence diffusion, wind speed, air pressure,
526 geopotential height patterns and their relation to haze and $PM_{2.5}$ were
527 evaluated and the results are summarized below.

528 The comparison between modeled AOD, SSA, and ASY data and MODIS,
529 CARSNET and AERONET observational data confirms the model's ability to
530 predict aerosol column loading and aerosol optical features, fundamental to
531 studying and evaluating the aerosols' radiative feedback to regional and local
532 PBL circulation. The modeled PBL wind speed correlates closely with the
533 NCEP analysis data, showing the model's ability to predict PBL wind speeds
534 as a base for haze forecasting. Modeled and observed AOD showed that the
535 monthly mean AOD values may exceed 1.2 and the daily mean value was
536 likely larger than 2.0 for the period 7–11 July, 2008 in the 3JNS Region. SSA is
537 as high as 0.90–0.96 and ASY is 0.72–0.74, showing the high scattering
538 properties of aerosols in summer. The PBL wind speed from modeled and
539 NCEP Reanalysis data both show a completely inverse trend with $PM_{2.5}$,
540 changing diurnally. This illustrates the importance of the "PBL window shadow"
541 to the haze episode. Low turbulence diffusion and PBL height are also
542 important meteorological factors affecting haze episodes, as evident from their
543 correlation with near-surface $PM_{2.5}$ either on a regional or a diurnal basis.

544 Contrary to the findings of most previous studies, a "homogeneous air
545 pressure pattern" appears not to be typical of the surface pressure field in
546 summer in middle and eastern China: surface pressure patterns are almost

identical for both a hazy day (July 10, 2008) and a clear day (12 July, 2008) after haze. The geopotential height patterns of the PBL (850–950 hPa) show a "homogeneous air pressure" field in middle and eastern China between the land-based, cold high over northwest China and Mongolia and the subtropical high over the East China Sea on a hazy day (10 July, 2008). The haze ended on 12 July, 2008 over eastern China, accompanied by an extension into midnorthern China of the land-based cold high from the northwest, and a weakening and easterly retrenchment to the east of the subtropical high. The PBL "homogeneous air pressure" over middle and eastern China was disrupted and cold air from Mongolia controlled midnorthern China at 850–950 hPa. This resulted in the wind speed increasing in middle and eastern China at this height. A downward momentum from the PBL (850–950 hPa) to the surface directly led to the surface wind increasing, and, combined with the PBL cold air, this resulted in the collapse of the hazy weather over eastern China.

Since all discussions above are based on the results from a haze episode in July 2008, any conclusions drawn concerning PBL meteorological and aerosol optical features during hazy weather may only apply to summer haze episodes. Haze episodes in other seasons need to be studied: the results may be different because of the different prevalent meteorological conditions in different seasons. In this study, aerosol optical parameters were calculated online, but their radiative effects were not entered online to the model's dynamical process. In the companion paper, aerosol radiative feedback and its impact on PBL meteorology and the haze episode itself will be implemented and discussed in detail.

Acknowledgments

This work is supported by the National Basic Research Program (973) (Grant Nos. 2011CB403404), the National Natural Scientific Foundation of China (Grant Nos. 41275007, 41130104, and 41475136), and CAMS Key Projects (Grant No. 2013Z007).

References

An, X. Q., Sun, Z. B., Lin, W. l., Jin, M., and Li, N.: Emission inventory evaluation using observations of regional atmospheric background stations of China, J. Environ. Sci., 25 (3), 537–546, 2013.

Chak K. C., and Yao, X. h.: Review Air pollution in mega cities in China, Atmos. Environ., 42, 1–42, 2008.

Cao, J. J., Lee, S. C., Ho, K. F., Zou, S. C., Fung, K., Li, Y., Watson, J. G., and Chow, J. C.: Spatial and seasonal variations of atmospheric organic carbon and elemental carbon in Pearl River Delta Region, Chin. Atmos. Environ., 38, 4447–4456, 2004.

Cao, G., Zhang, X., and Zheng, F.: Inventory of black carbon and organic carbon 446 emissions from China, Atmos. Environ., 40, 6516–27, 2006.

Cao, G. L.， AN, X. Q., Zhou C. H., Ren, Y. Q., and Tu, J.: Emission inventory of air pollutants in China, Chin. Environ., Sci., 30 (7),900~906, 2010.

Chan, C. Y., Tang, J. H., Li, Y. S., and Chan, L. Y.: Mixing ratios and sources of halocarbons in urban, semi-urban and rural sites of the Pearl River Delta, South China, Atmos. Environ., 40, 7331–7345, 2006.

Che, H., Zhang, X., Chen, H., Damiri, B., Goloub, P., Li, Z., Zhang, X., Wei, Y., Zhou, H., Dong, F., Li, D., and Zhou, T.: Instrument calibration and Aerosol Optical Depth (AOD) validation of the China Aerosol Remote Sensing Network (CARSNET), J. Geophys. Res., 114. doi:10.1029/2008JD011030, 2008.

Che, H. Z., Zhang, X. Y., and Li, Y.: Haze trends over the capital cities of 31 provinces in China, 1981-2005, Theor. App. Clim., 97, 235-242, 2009.

Che, H., Xia, X., Zhu, J., Li, Z., Dubovik, O., Holben, B., Goloub, P., Chen, H., Estelles, V., Cuevas-Agulló, E., Blarel, L., Wang, H., Zhao, H., Zhang, X., Wang, Y., Sun, J., Tao, R., Zhang, X., and Shi, G.: Column aerosol optical properties and aerosol radiative forcing during a serious haze-fog month over North China Plain in 2013 based on ground-based sunphotometer measurements, Atmos. Chem. Phys., 14, 2125-2138,

607 doi:10.5194/acp-14-2125-2014, 2014.
608 Chen, D. H., Xue, J. S., and Yang, X. S.: The new generation of
609 hydrostatic/nonhydrostatic multi-scales numerical prediction model:
610 Scientific design and experiments (in Chinese), CAMS Technical Report 1.,
611 2003.
612 Chen, D. H, Xue, J. S., Yang, X. S., Zhang, H. L., Shen, X. S., Hu, J. L., Wang,
613 Y., Ji , L. R., Chen, J. B.: (New generation of multi-scale NWP system
614 (GRAPES): general scientific design, Chin. Sci. Bull., 53(22), 3433-3445,
615 2008.
616 Chen, Z. H., Cheng, S. Y., and Su, F. Q.: Analysis of large-scale weather
617 pattern during heavy air pollution process in Beijing), Res. Environ. Sci. (in
618 Chinese), 20 (2), 99-105, 2007.
619 Cheng, Y., Canuto, V. M., and Howard, A. M.: An improved model for the
620 turbulent PBL, J. Atmos. Sci., 59, 1550–1565, 2002.
621 Chou, M. D., Suarez, M. J., Ho, C. H., Yan, M. M. H., and Lee, K. T.:
622 Parameterizations for Cloud Overlapping and Shortwave Single-Scattering
623 Properties for Use in General Circulation and Cloud Ensemble Models, J.
624 Clim., 11, 202–214, 1998.
625 Chou, M. D., Suarez, M. J., Liang, X. Z., and Michael M.-H. Y.: A Thermal
626 Infrared Radiation Parameterization for Atmospheric Studies, Technical
627 Report Series on Global Modeling and Data Assimilation,
628 NASA/TM-2001-104606, 19, America, Goddard Space Flight Center,
629 Greenbelt, Maryland, 55, 2001.
630 Duan, J. C., Guo, S. J., Tan, J. H., Wang, S., and Chai, F. H. : a Characteristics
631 of atmospheric carbonyls during haze days in Beijing, China, Atmos. Res.,
632 114-115, 17-27, 2012.
633 Fu, Q. Y., Zhuang, G. S., Wang, J., Xu, C., Huang, K., Li, J., Hou, B., Lu, T.,
634 and Streets, D. G.: Mechanism of formation of the heaviest pollution
635 episode ever recorded in the Yangtze RiverDelta, China, Atmos. Environ.
636 42, 2023–2036, 2008.

637 Gao, J., Wang, T., Zhou, X. H., Wu, W. S., and Wang, W. X.: Measurement of
638 aerosol number size distributions in the Yangtze River delta in China:
639 formation and growth of particles under polluted conditions, Atmos.
640 Environ., 43, 829–836, 2009.
641 Gao, L. N., Jia, G. S., Zhang, R. J., Che, H. Z., Fu, C. B., Wang, T. J., Zhang, M.
642 G., and Jiang, H.: Visibility trends in the Yangtze River Delta of China
643 during 1981-2005, J. Air. Waste. Manage., 61, 843-849, 2011.
644 Gong, S. L, and Zhang, X. Y.: CUACE/Dust – an integrated system of
645 observation and modeling systems for operational dust forecasting in Asia,
646 Atmos. Chem. Phys., 8, 2,333-82,340, 2008.
647 Hess, M., Koepke, P., and Schult, I., Optical Properties of Aerosols and Clouds:
648 The software package OPAC, Bull. Am. Met. Soc., 79, 831-844, 1998.
649 Hong, S. Y. and Pan, H. L.: Nonlocal boundary layer vertical diffusion in a
650 Medium-Range Forecast model, Mon. Weather Rev., 124, 2322–2339,
651 1996.
652 Hong, S. Y., Noh, Y., and Dudhia, J.: A new vertical diffusion package with an
653 explicit treatment of entrainment processes, Mon. Wea. Rev., 134,
654 2318–2341, 2006.
655 Huang, J., Lin, B., Minnis, P., Wang, T., Wang, X., Hu, Y., Yi, Y., and Ayers, J.:
656 Satellite-based assessment of possible dust aerosols semi-direct effect on
657 cloud water path over East Asia, Geo. Res. Let., 33 (19), L19802,
658 doi:10.1029/2006GL026561, 2006.
659 Huang, J. P., Zhang, W., Zuo, J. Q., Bi, J. R., Shi, J. S., Wang, X., Chang, Z. L.,
660 Huang, Z. W., Yang, S., Zhang, B. D., Wang, G. Y., Feng, G. H., Yuan, J. Y.,
661 Zhang, L., Zuo, H. C., Wang, S. G., Fu, C. B., and Chou, J. F. : An overview
662 of the semi-arid climate and environment research observatory over the
663 Loess Plateau. Adv. Atmos. Sci., 25(6), 906–921, 2008.Huang, J., Wu, D.,
664 Huang, M. H., Li, F., Bi, X. Y., Tan, H. B., and Deng, X. J.: Visibility
665 variations in the Pearl River delta of China during the period of 1954–2004,
666 J. App. Meteor., 19, 61–70, 2008.

667 Huang, J., Fu, Q., Su, J., Tang, Q., Minnis, Y., Hu, P., Yi, Y., and Zhao, Q.:
668 Taklimakan dust aerosol radiative heating derived from CALIPSO
669 observations using the Fu-Liou radiation model with CERES constraints,
670 Atmos. Chem. Phys., 9 (12), 2009.
671 Hsu, N. C., Si-Chee, T., King, M. D., and Herman, J. R., : Deep Blue Retrievals
672 of Asian Aerosol Properties During ACE-Asia, Geoscience and Remote
673 Sensing, IEEE Transactions on, 44(11), 3180-3195, 2006.
674 Ichoku, C., Chu, D.A., Mattoo, S., Kaufman, Y.J., Remer, L.A., Tanré, D.,
675 Slutsker, I., and Holben, B.N.: A spatio-temporal approach for global
676 validation and analysis of MODIS aerosol products, Geophys. Res. Let.,
677 29 (12), 8006. doi:10.1029/2001GL013206, 2002.
678 Kang H. Q., Zhu, B., Su, J. F., Wang, H. L., Zhang, Q. C., and Wang, F. :
679 Analysis of a long-lasting haze episode in Nanjing, China, Atmos. Res.,
680 78-87, 2013.
681 Kahn, R., Garay, M., Nelson, D., Yau, K., Bull, M., and Martonchik, J.:
682 Satellitederived aerosol optical depth over dark water from MISR and
683 MODIS: comparisons with AERONET and implications for climatological
684 studies. J. Geophys. Res., 112, D18205, doi:10.1029/2006JD008175,
685 2007.
686 Kessler, E.: On the distribution and continuity of water substance in
687 atmospheric circulation, Meteor. Monogr., 32, Amer. Meteor. Soc., 84pp,
688 1969.
689 Kain, J. S.: The Kain-Fritsch convective parameterization: An update, J. Appl.
690 Meteor., 43, 170–181, 2004.
691 Kusaka, H., Kondo, H., Kikegawa, Y., Kimura, F.: A simple single-layer urban
692 canopy model for atmospheric models: Comparison with multi-layer and
693 slab models. Bound.-Layer Meteor., 101, 329–358, 2001.
694 Lee,Y. L., and Sequeira, R.: Visibility degradation across Hong Kong: its
695 components and their relative contributions, Atmos. Environ., 34,
696 5861–5872, 2001.

Liu, X. H., Zhang, Y., Cheng, S. H., Xing, J., Zhang, Q., Streets, D. G., Jang, C., Wang, W. X., and Hao, J. M.: Understanding of regional air pollution over China using CMAQ, part I performance evaluation and seasonal variation, Atmos. Environ., 44, 2415-2426, 2010.

Liu W. D., Jiang, Y. H., and Li, J.: Characteristics of aerosol distribution and transmission of a heavy air pollution process in Beijing area, Clim. Environ. Res. (in Chinese), 15 (2), 152- 160, 2010.

Pleim, J. : A combined local and non-local closure model for the atmospheric boundary layer. Part II: Application and evaluation in a mesoscale meteorological model, J. Applied Meteor. Climatology, 46, 1396–1409, 2007.

Quan. J., Tie, X., Zhang., Q., and Liu, Q.: Characteristics of heavy pollution during the 2012-2013 winter in Beijing, China. Atmos. Envoirn., 88, 83-89, 2014.

Rothman, L.S., Gordon, I.E., Barbe, A., Chris Benner, D., ,Bernath, P.F., Birk, M., ,Boudon, V., Brown, L.R., Campargue, A., Champion, J.P., Chance, K., Coudert, L.H., Dana, V., ,Devi, V.M., Fally, S., Flaud, J.-M., Gamache, R.R., Goldman, A., Jacquemart, D., Kleiner, I., Lacome, N., Lafferty, W.J., Mandin, J.-Y., ,Massie, S.T., Mikhailenko, S.N., Miller, C.E., Moazzen-Ahmadi, N., Naumenko, O.V., Nikitin, A.V., Orphal, J., Perevalov, V.I., Perrin, A., Predoi-Cross, A., Rinsland, C.P., Rotger, M., Šimečková, M., Smith, M.A.H., Sung, K., Tashkun, S.A., Tennyson, J., Toth, R.A., Vandaele, A.C. and Vander Auwera, J.: The HITRAN 2008 molecular spectroscopic database, J. Quant. Spect. and Rad. Trans., 110 (9-10), 533-572, 2009.

Remer, L. A., Kaufman, Y. J., Tanre, D., Mattoo, S., Chu, D. A., Martins, J. V., Li, R. R., Ichoku, C., Levy, R. C., Kleidman, R. G., Eck, T. F., Vermote, E., Holben, B. N.: The MODIS Aerosol Algorithm, Products, and Validation, J. Atmos. Sci., 66, 947-973, 2005.

Santanello, J. A., Friedl, M. A., and Kustas, W. P. : An empirical investigation of convective planetary boundary layer evolution and its relationship with the

727 land surface, J. Applied Meteor., 44, 917–932, 2005.
728 Stockwell, W. R., Middleton, P., Chang, J. S., Tang X.: The Second Generation
729 Regional Acid Deposition Model Chemical Mechanism for Regional Air
730 Quality Modeling, J. Geophys. Res. 95, 16343- 16376,1990.
731 Tan, J., Duan, J., Chen, D., Wang, X., Guo, S., Bi, X., Sheng, G., He, K., and
732 Fu, J. : Chemical characteristics of haze during summer and winter in
733 Guangzhou, Atmos. Res., 94, 238-245, 2009.
734 Tan, J., Guo, S. J., Ma, Y. L., Duan, J. C., Cheng., Y., He., K. B., and Yang, F.
735 M.: Characteristics of particulate PAHs during a typical haze episode in
736 Guangzhou, China, Atmos. Res., 102, 91-98, 2011.
737 Vogelezang, D. H. P., and Holtslag, A. A. M. : Evaluation and model impacts of
738 alternative boundary-layer height formulations, Bound. Layer Meteor., 81,
739 245-269, doi:10.1007/BF02430331, 1996.
740 Wang, L. T., Hao, J. M., and He, K. B.: A modeling study of coarse particulate
741 matter pollution in Beijing: regional source contributions and control
742 implications for the 2008 Summer Olympics, J. Air. Waste. Mnanage., 58,
743 1057e1069. doi:10.3155/1047-3289.58.8.1057, 2008.
744 Wang, L. T., Xu, J., Yang, J., Zhao, X. J., Wei, W., Cheng, D. D., Pan, X. M.,
745 and Su, J.: Understanding haze pollution over the southern Hebei area of
746 China using the CMAQ model, Atmos. Environ., 56, 69-79, 2012.
747 Wang, H., Shi, G. Y., Aoki, T., Wang, B., and Zhao, T. L.: Radiative forcing due
748 to dust aerosol over east Asia-north Pacific region during spring 2001，
749 Chin. Sci. Bull., 49(20), 2212-2219, 2004.
750 Wang, H., Shi, G. Y., Li., W., and Wang, B.: The impacts of optical properties on
751 radiative forcing due to dust aerosol, Adv. Atmos. Sci., 23（2），431- 441,
752 2006.
753 Wang, H., Gong, S. L., Zhang, H. L., Chen, Y., Shen, X. S., Chen, D. H., Xue, J.
754 S., Shen, Y. F., Wu, X. J., and Jin, Z. Y.: A new-generation sand and dust
755 storm forecasting system GRAPES_CUACE/Dust: Model development,
756 verification and numerical simulation. Chin. Sci. Bull, doi:

10.1007/s11434-009-0481-z, 2009.

Wang, H., Zhang, X. Y., Gong, S., Chen, Y., Shi, G., and Li, W.: Radiative feedback of dust aerosols on the East Asian dust storms, J. Geophys. Res., 115, D23214, doi:10.1029/2009JD013430, 2010.

Wang H., Tan, S. C., Wang, Y., Jiang, C., Shi, G. Y., Zhang M., Che, H. Z.: A multisource observation study of the severe prolonged regional haze episode over eastern China in January 2013. Atmos. Environ., 89, 807-815, 2014a.

Wang, H., Xu, J. Y., Zhang, M., Yang, Y. Q., Shen, X., J., Wang, Y. Q., Chen, D., Guo, J. P.: A study of the meteorological causes of a prolonged and severe haze episode in January 2013 over central-eastern China, Atmos. Environ., 98, 146-157, 2014b.

Wang, T. J., Jiang, F., Deng, J. J., Shen, Y., Q., Fu, Y., Wang, Q., Fu, Y., Xu, J. H.: Urban air quality and regional haze weather forecast for Yangtze River Delta region, Atmos. Environ., 58, 70-83, 2012.

Wang, Y., Zhuang, G., Sun, Y., and An, Z. : The variation of characteristics and formation mechanisms of aerosols in dust, haze, and clear days in Beijing, Atmos. Environ., 40, 6579 – 6591, 2006.

Wang, Y. T., Li, W.，Zhang X. L., and Meng, W.: Relationship between atmospheric boundary layer and air pollution in summer stable weather in the Beijing urban area［J］. Res. Environ. Sci.，25 (10),1092-1098, 2012.

Wei, W. X., Zhang, X., and Tian, G. Q.: Analysis of relation between haze distribution and terrain and wind speed in Hebei Province, J. Nat. Disasters (in Chinese), 19 (1), 49-52, 2010.

Westerdahl, D., Wang, X., Pan, X., and Zhang, K. M.: Characterization of on-road vehicle emission factors and microenvironmental air quality in Beijing, China. Atmos. Environ., 43(3), 697-705, 2009.

Wu, Z. J., Hu, M., Lin, P., Liu, S., Wehner, B., and Wiedensohler, A. : Particle number size distribution in the urban atmosphere of Beijing, China. Atmos. Environ. 42, 7967–7980, 2008.

787 Wu, D., Tie, X. X., Li, C. C., Ying, Z. M., Lau, A. K., Huang, J., Deng, X. J., Bi, X.
788 Y. : An extremely low visibility event over the Guangzhou region: a case
789 study, Atmos. Environ., 39, 6568–6577, 2006.
790 Wu, D., Wu, X. J., and Li, F.: Temporal and spatial variation of haze during
791 1951-2005 in Chinese mainland, Acta. Meteor. Sinica. (in Chinese), 68,
792 680-688, 2010.
793 Xing, J., Zhang, Y., and Wang, S. X. : Modeling study on the air quality impacts
794 from emission reductions and a typical meteorological conditions during
795 the 2008 Beijing Olympics, Atmos. Environ., 45, 1786-1798, 2011.
796 Xu, G. Q, Chen, D. H, and Xue, J.S.: The program structure designing and
797 optimizing tests of GRAPES physics, Chin Sci Bull, 2008, 53(22),
798 3470-3476, 2008.
799 Yang, S., Guang, Y. S., Chen, L., Wang, B., Yang, H. L.: Evaluation of
800 Moderate-Resolution Imaging Spectroradiometer (MODIS) Deep Blue
801 Aerosol Products Using Ground-Based Measurements over Beijing, SOLA,
802 7, 133−136, doi:10.2151/sola.2011-034, 2011.
803 Yang, X. S., Chen, J. B., and Hu, J. L.: A semi-implicit semi-Lagran global
804 nonhydrostatic model and the polar discretization scheme, Sci. China Ser
805 D-Earth Sci., 2007, 50(2),1885-1891, 2007.
806 Yin, Y., Tong, Y. Q., Wei, Y. X., Wang, T. J., Li, J. P., Yang, W. F., and Fan, S. X.:
807 The analysis of chemistry composition of fine-mode particles in Nanjing,
808 Trans, Atmos. Sci., 32 (6), 723–733 (in Chinese), 2009.
809 Zhang, M., Uno, I., and Yoshi, Y.: Transport and transformation of sulfur
810 compounds over East Asia during the TRACE-P and ACE-Asia campaigns,
811 Atmos. Environ., 38, 6947-6959, 2004.
812 Zhang, R. H., and Shen, X. S.: On the development of the GRAPES—A new
813 generation of the national operational NWP system in China. Chin. SCI.
814 Bull., 53(22), 3429－3432, 2008.
815 Zheng, M., and Fang, M.: Particle-associated polycyclic aromatic
816 hydrocarbons in the atmosphere of Hong Kong, Water. Air and Soil

817 Pollution, 117, 175–189, 2000.
818 Zhang, J., and Reid, J.S.: A decadal regional and global trend analysis of the
819 aerosol optical depth using a data-assimilation grade over-water MODIS
820 and Level 2MISR aerosol products. Atmos. Chem. Phys, 10, 10949-10963,
821 2010.
822 Zhang, X. Y., Wang, Y. Q., and Lin, W. L.: Changes of atmospheric composition
823 and optical properties over Beijing 2008 Olympic monitoring Campaign,
824 BAMS, 1634–1651, 2009.
825 Zhang, X. Y., Zhang Y. F.， Feng, Y. C., Han, S. Q., Han, B.， LI, L.， XU, H.:
826 Influence of Synoptic Patterns on the Concentrations of PM10 in Tianjin,
827 Res. of Environ. Sci. (in Chinese), 23(9), 1115-1116, 2013.
828 Zhang, Y. M., Zhang, X. Y, Sun, J. Y.: Characterization of new particle and
829 secondary aerosol formation during summertime in Beijing, China, Tellus,
830 63, 382–394, 2011.
831
832

833 Figure captions

834 Fig. 1 The (a) mass extinction coefficient, Kext (m^2 g), (b) SSA, and (c) ASY for
835 six of the 12 model size bins for seven species of dry aerosols.

836 Fig. 2 The (a) mass extinction coefficient, Kext (m^2 g), (b) SSA, and (c) ASY of
837 typical particle size (the red line in Fig. 1) for five hygroscopic aerosol species
838 at six different rh.

839 Fig. 3 Monthly mean MODIS (topup) and modeled AOD (bottom) for July 2008.

840 Fig. 4 Daily variation of CRASNET observations (Obs.) and model-derived
841 (Model) AOD from 1 to 31 July, 2008.

842 Fig. 5 Vertical distribution of atmospheric particle pollutants: (a) daily variations
843 of 3JNS-the mean PM2.5 (μg m^{-3}) from 1 to 31 July, 2008; (b) the averaged
844 extinction coefficient (K_{EXT}) (m^2 g^{-1}, left) and PM2.5 (right) for 7–11 July, 2008
845 for the 3JNS region.

846 Fig. 6 Daily changes of the 3JNS mean wind speeds (m s^{-1}) derived from the
847 model and NCEP Reanalysis 2, together with simulated PM2.5 (μg m^{-3}) at
848 850–950 hPa (Fig. 6a) and at the surface (Fig 6b).

849 Fig. 7 Mean surface PM2.5 (μg m^{-3}, contour) and fktm (m^2 s^{-1}, shaded) for
850 7–11 July, 2008 (top) and the daily changes of the 3JNS mean PM2.5 and fktm
851 for 1–31 July, 2008 (bottom).

852 Fig. 8 The mean surface PM2.5 (μg m^{-3}, contours) and PBL height (m, shaded)
853 for 7–11 July, 2008 (top), and daily changes of the 3JNS mean surface PM2.5
854 and PBL height (bottom).

855 Fig. 9 Air pressure patterns (hPa, shaded), wind vectors at the surface (m s^{-1},
856 bottom), geopotential height (gph, shaded), wind vector at 950 hPa (middle)
857 and 850 hPa (top) on 10 July (left) and 12 July, 2008 (right).

858

Table 1 Configured GRAPES_CUACE options for physical processes

Physical process	Configured options	References
Longwave radiation	Goddard	Chou et al., 2001
Shortwave radiation	Goddard	Chou et al., 1998
Cumulus clouds	KFETA Scheme	Kain, 2004
Surface Layer	SFCLAY Scheme	Pleim, 2007
Boundary layer	MRF Scheme	Hong and Pan, 1996
Land surface	SLAB Scheme	Kusaka et al., 2001
Cloud microphysics	KESSLER Scheme	Kessler, 1969
Gas-phase chemistry	RADM II	Stockwell et al., 1990
Aerosol chemistry	CUACE	Gong and Zhang, 2008

Table 2 CARSNET and AERONET station locations

Stations	Lat.	Long.	Altitude(m)
Beijing	39.80	116.47	31.3
Xianghe (AERONET)	39.76	117.00	
Datong	40.10	113.33	1067.2
Lanzhou	36.05	103.88	1517.2
SOCAL (AERONET)	35.57	104.08	
Shangdianzi	40.65	117.12	293.3
Longfengshan	44.73	127.60	330.5
Gucheng	39.13	115.80	15.1

Table 3 Observed and Modeled SSA, ASY and Model Bias

Station	Parameters	Obs.(times)	Model	Model Bias
Xianghe	SSA	0.96(10)	0.93	−3%
	ASY	0.74(10)	0.78	5%
SOCAL	SSA	0.95 (7)	0.90	−5%
	ASY	0.72(17)	0.77	7%

Fig. 1 The (a) mass extinction coefficient, K_{ext} (m^2 g), (b) SSA, and (c) ASY for six of the 12 model size bins for seven species of dry aerosols.

(a)

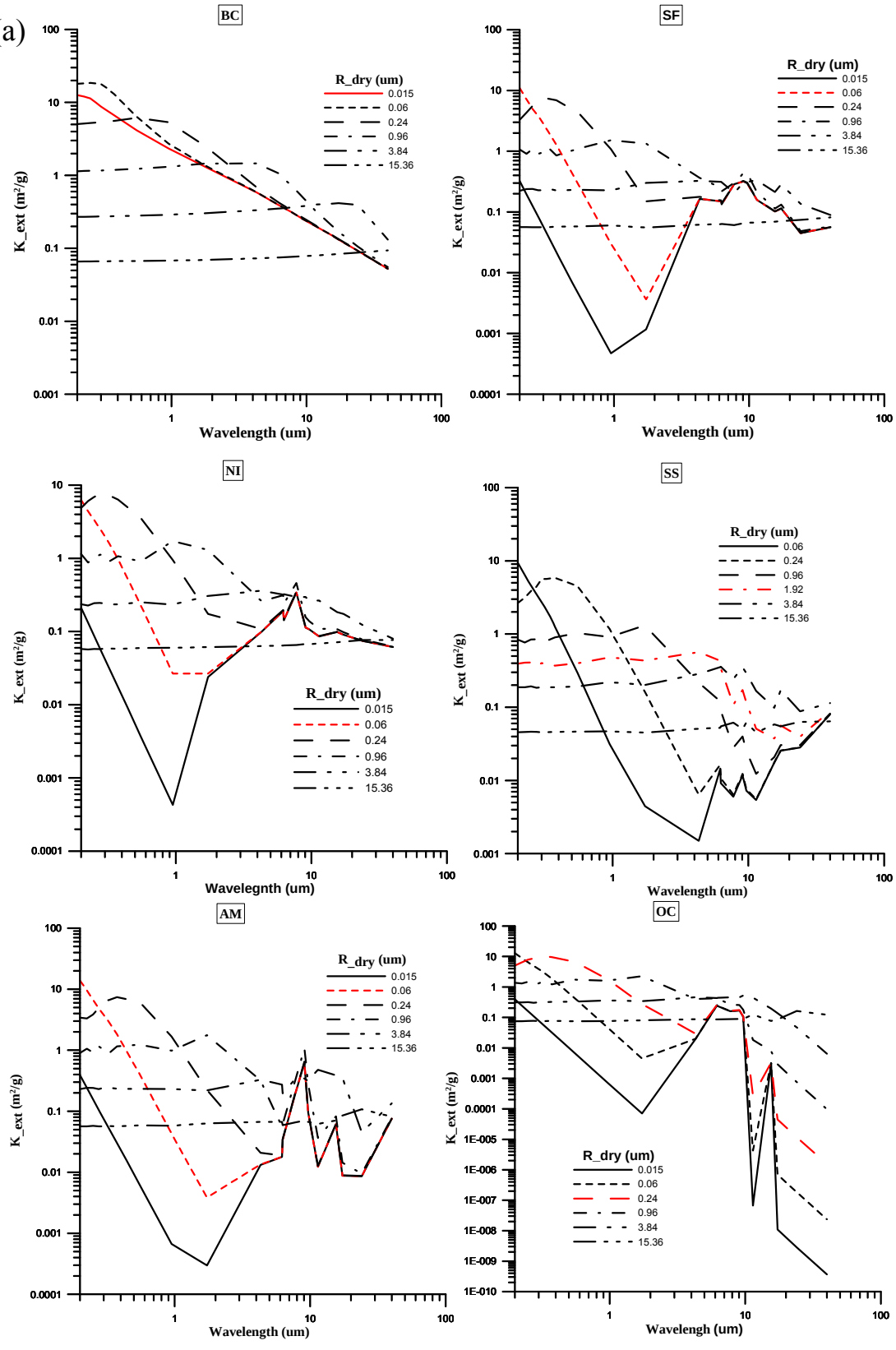

882

883

884

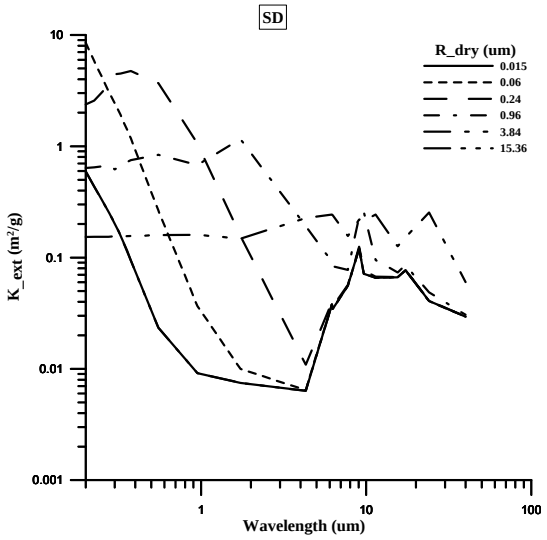
SD
R_dry (um)
0.015
0.06
0.24
0.96
3.84
15.36
K_ext (m²/g)
10
1
0.1
0.01
0.001
1
10
100
Wavelength (um)

(b)

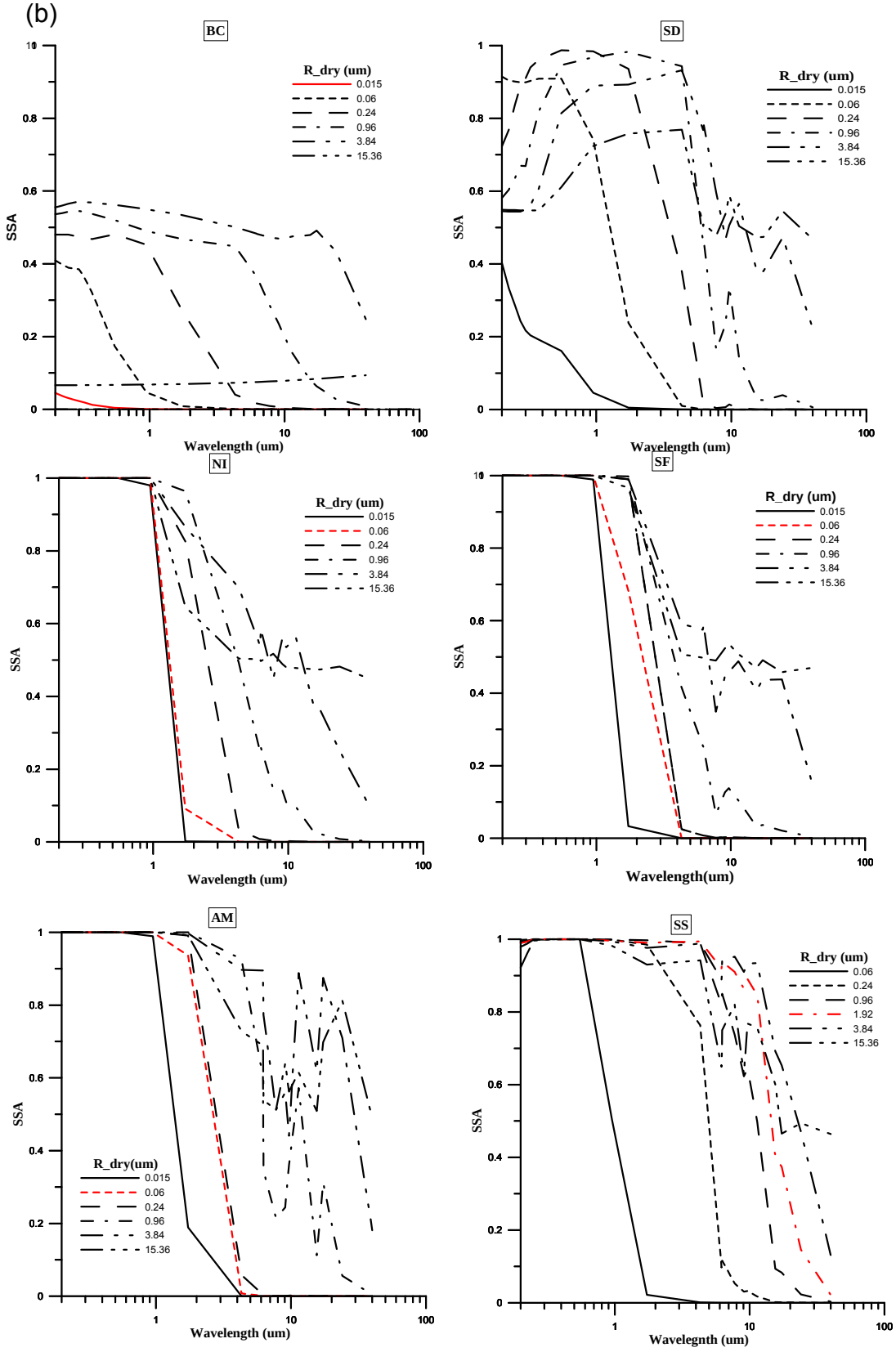
BC
SD
NI
SF
AM
SS
SSA
Wavelength (um)
Wavelength(um)
Wavelegnth (um)
R_dry (um)
R_dry(um)
0.015
0.06
0.24
0.96
1.92
3.84
15.36

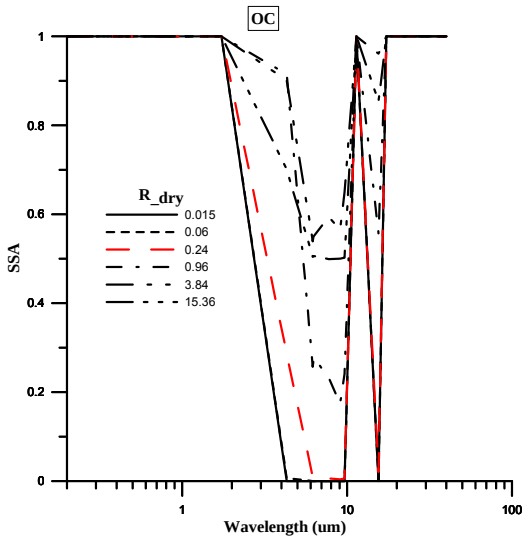
OC
SSA
Wavelength (um)
R_dry
0.015
0.06
0.24
0.96
3.84
15.36
0
0.2
0.4
0.6
0.8
1
1
10
100

(c)

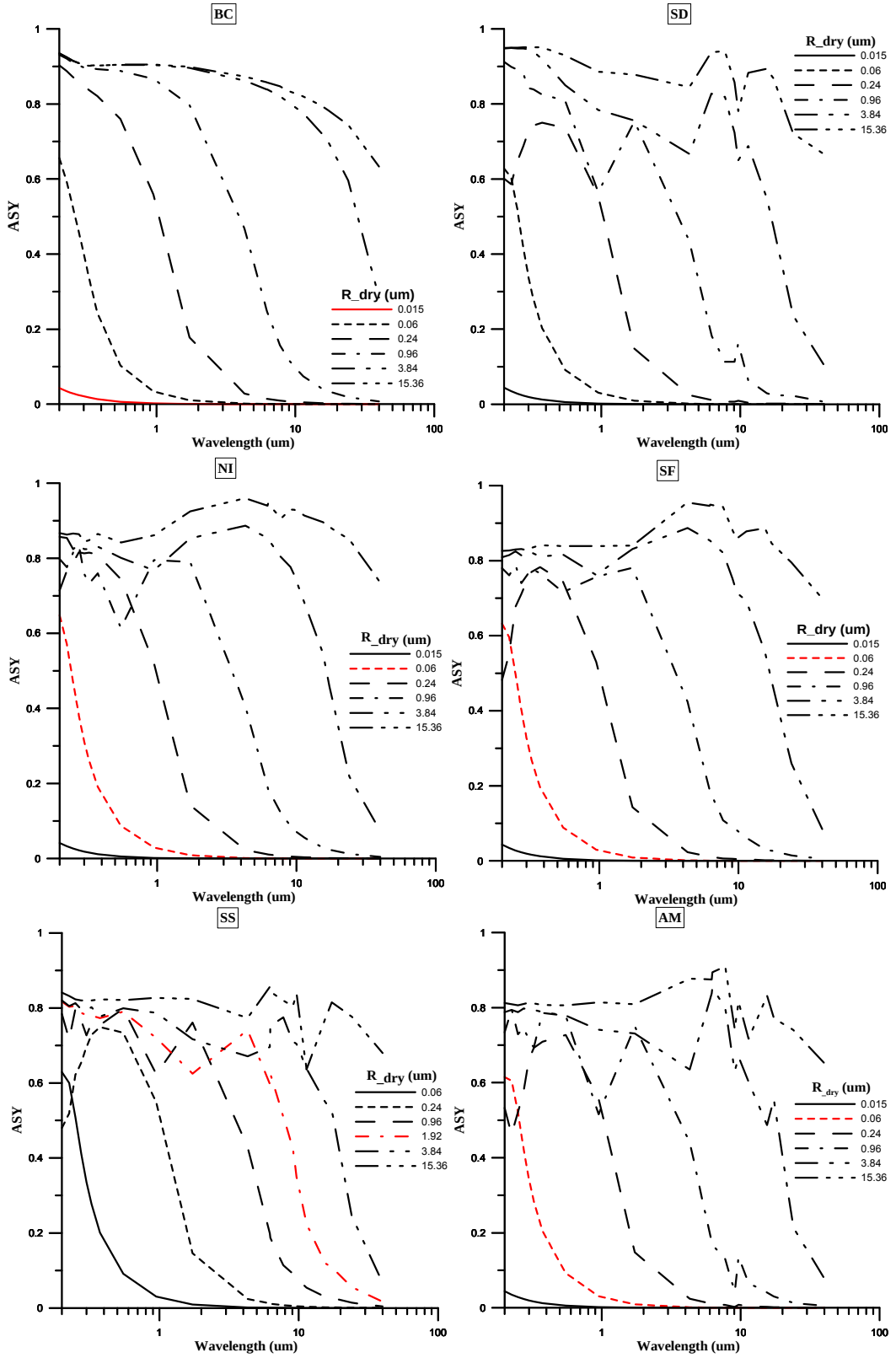
BC
SD
NI
SF
SS
AM
ASY
Wavelength (um)
R_dry (um)
0.015
0.06
0.24
0.96
1.92
3.84
15.36

933

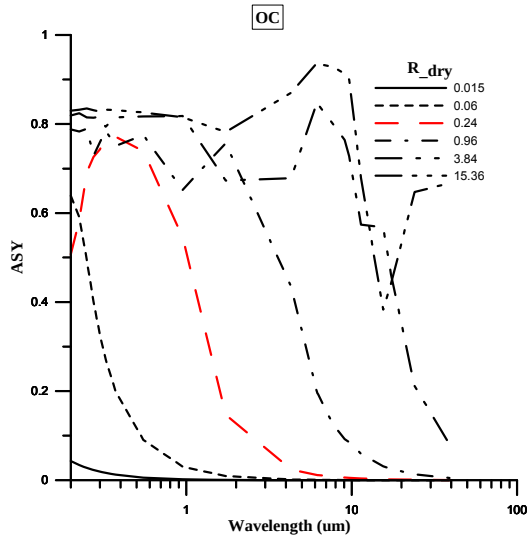
OC
R_dry
0.015
0.06
0.24
0.96
3.84
15.36
ASY
Wavelength (um)
0
0.2
0.4
0.6
0.8
1
1
10
100

Fig. 2 The (a) mass extinction coefficient, K_{ext} (m^2 g), (b) SSA, and (c) ASY of typical particle size (the red line in Fig. 1) for five hygroscopic aerosol species at six different *rh.*

(a)

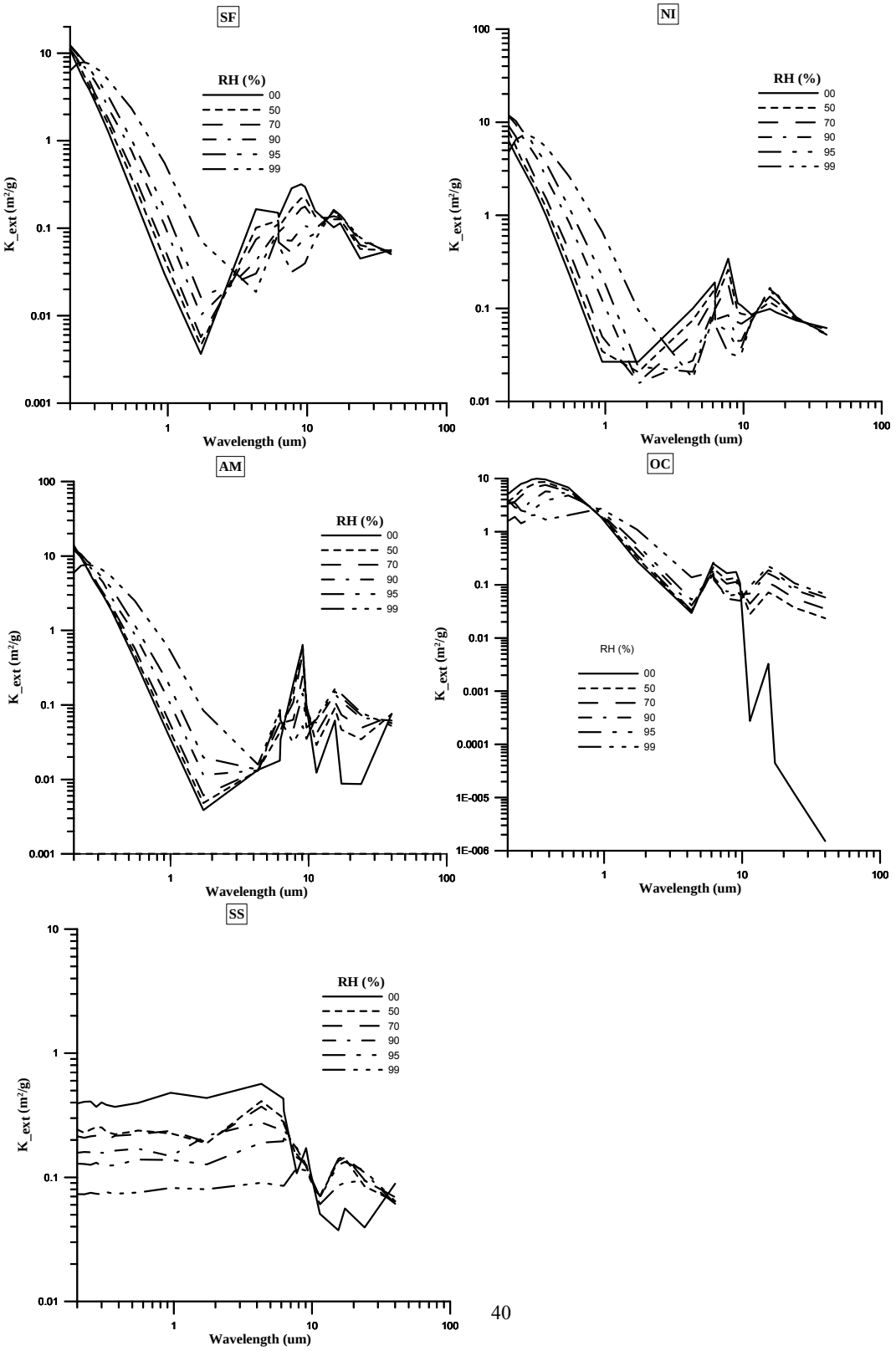

941 (b)

942

943

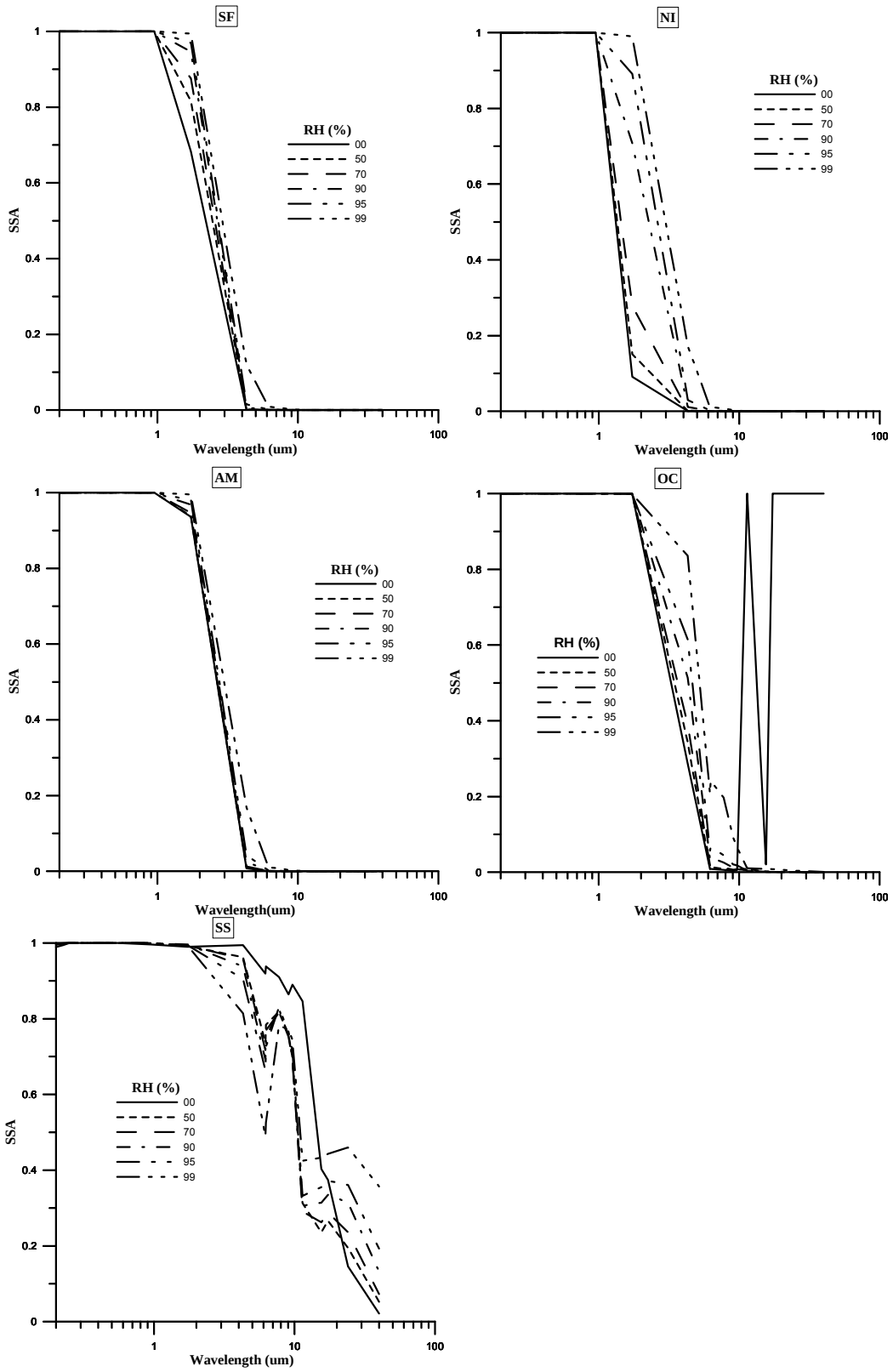
SF
NI
AM
OC
SS
SSA
Wavelength (um)
Wavelength(um)
RH (%)
00
50
70
90
95
99

944 (c)

945

946

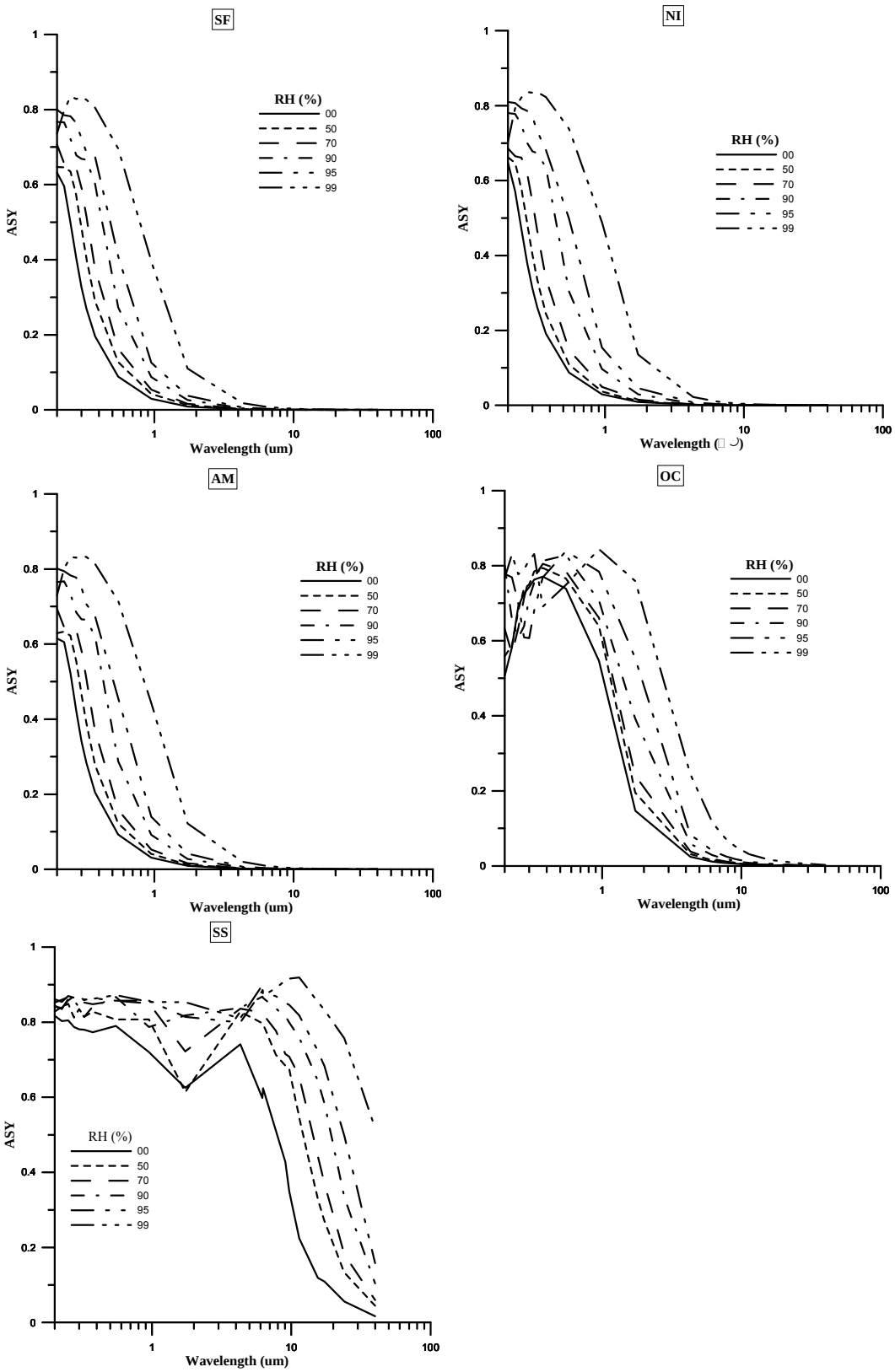

Fig. 3 Monthly mean MODIS (top) and modeled AOD (bottom) for July 2008.

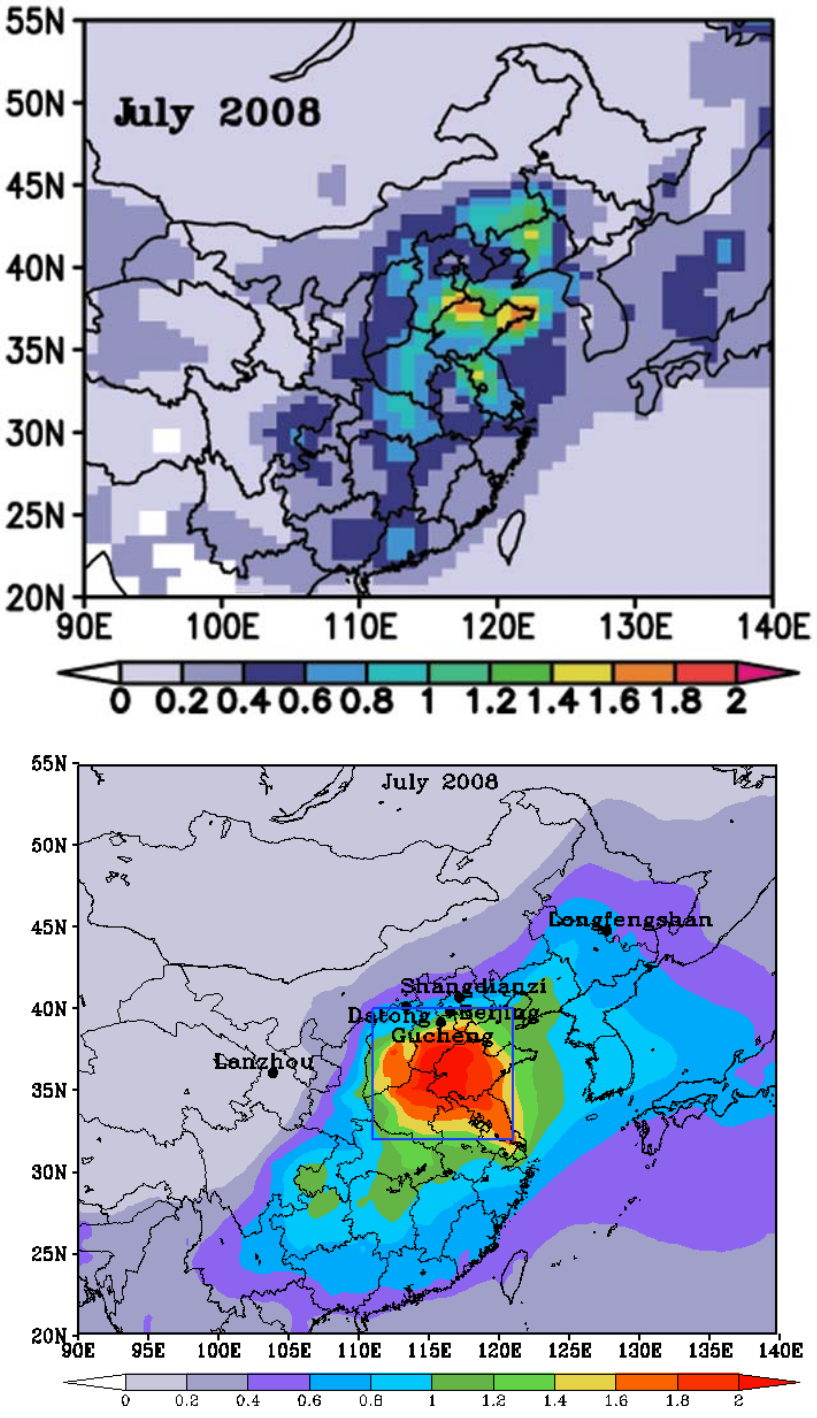

Fig. 4 Daily variation of CRASNET observations (Obs.) and model-derived (Model) AOD from 1 to 31 July, 2008.

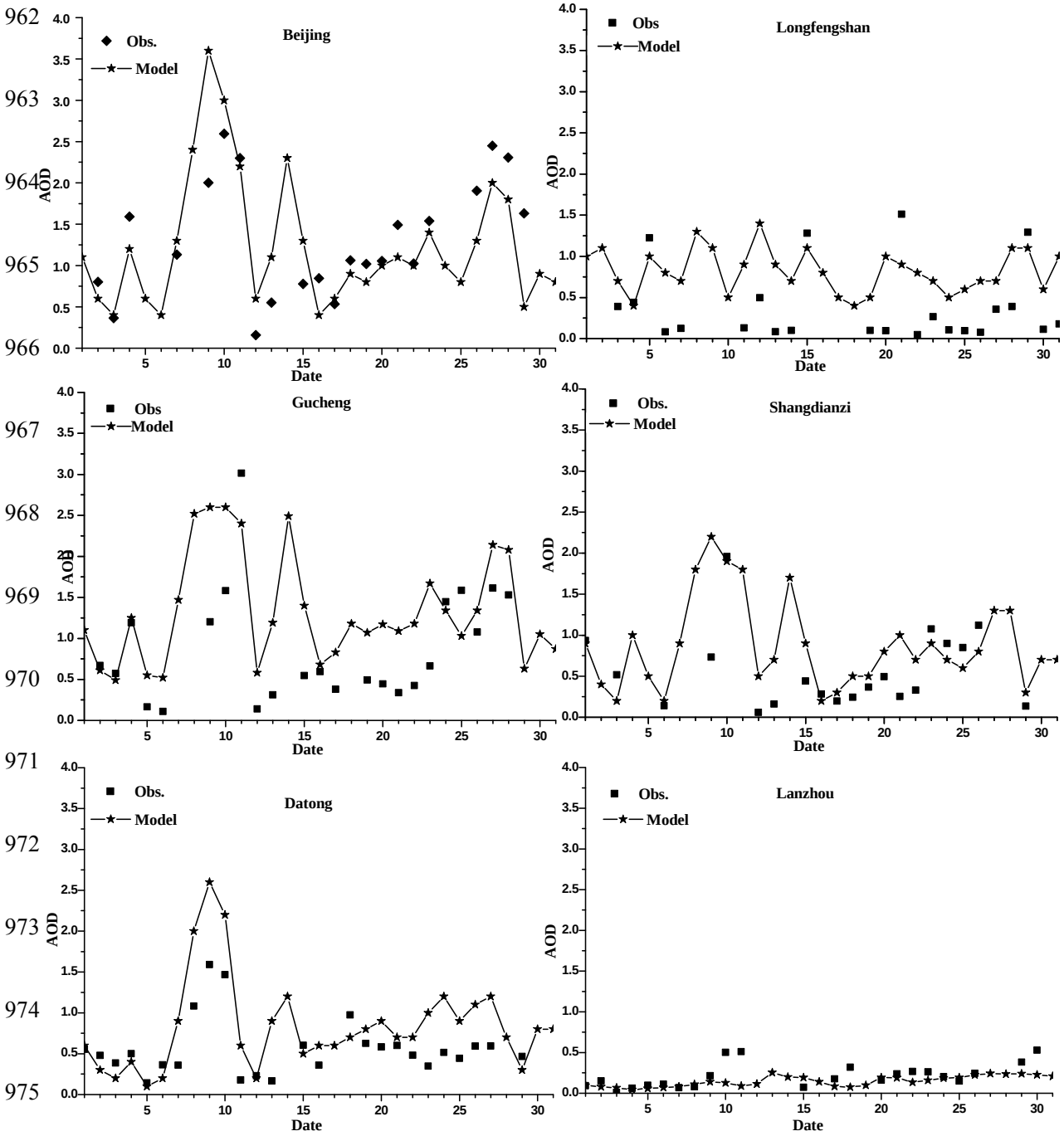

Fig. 5 Vertical distribution of atmospheric particle pollutants: (a) daily variations of 3JNS-the mean $PM_{2.5}$ (μg m^{-3}) from 1 to 31 July, 2008; (b) the averaged extinction coefficient (K_{EXT}) (m^2 g^{-1}, left) and $PM_{2.5}$ (right) for 7–11 July, 2008 for the 3JNS region.

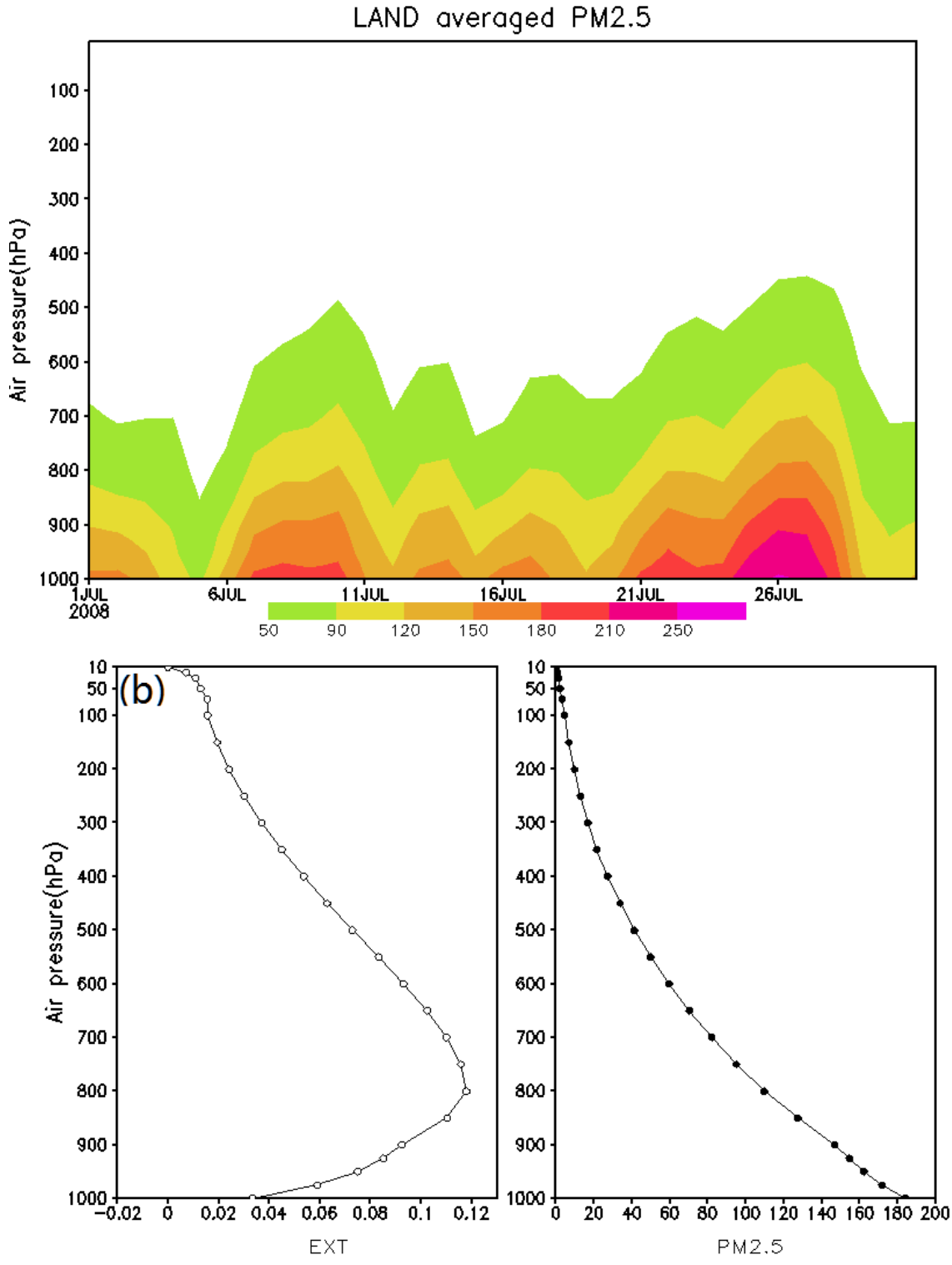

993 Fig. 6 Daily changes of the 3JNS mean wind speeds (m s^{-1}) derived from the
994 model and NCEP Reanalysis 2, together with simulated $PM_{2.5}$ (μg m^{-3}) at
995 850–950 hPa (Fig. 6a) and at the surface (Fig 6b).

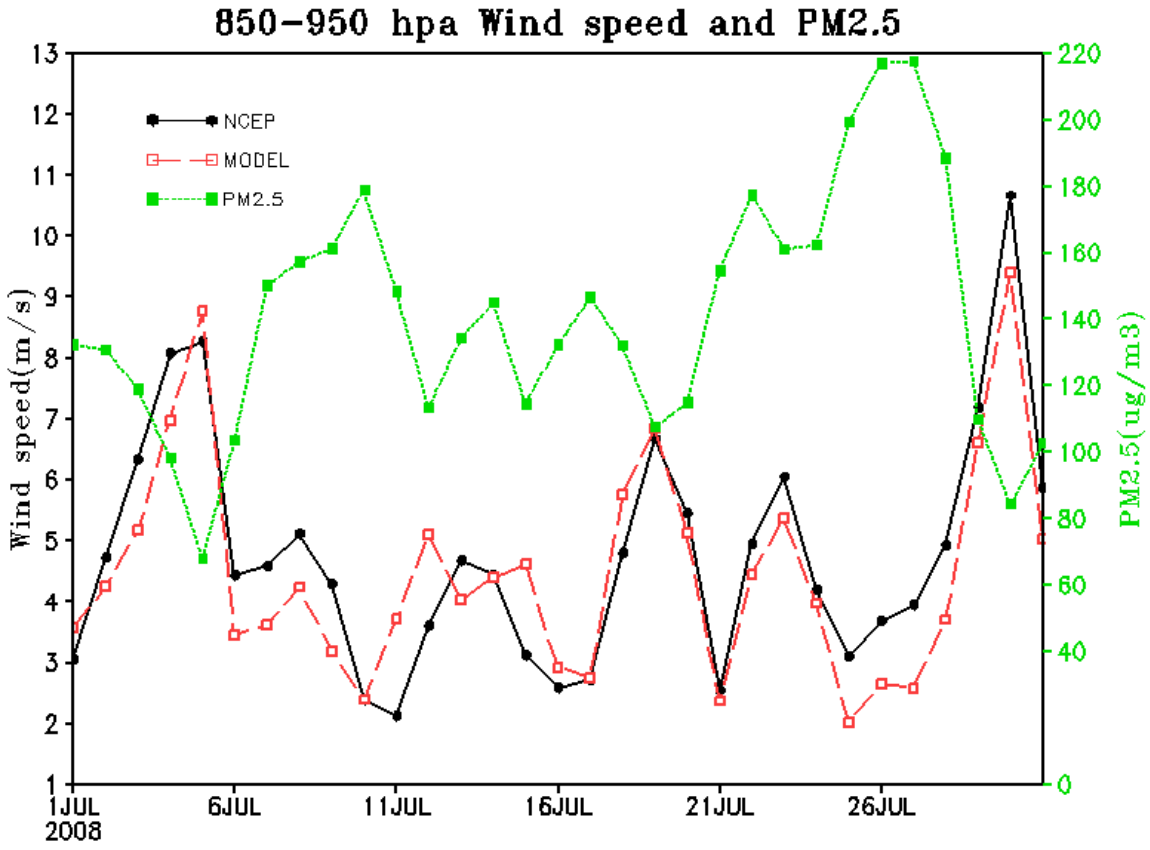

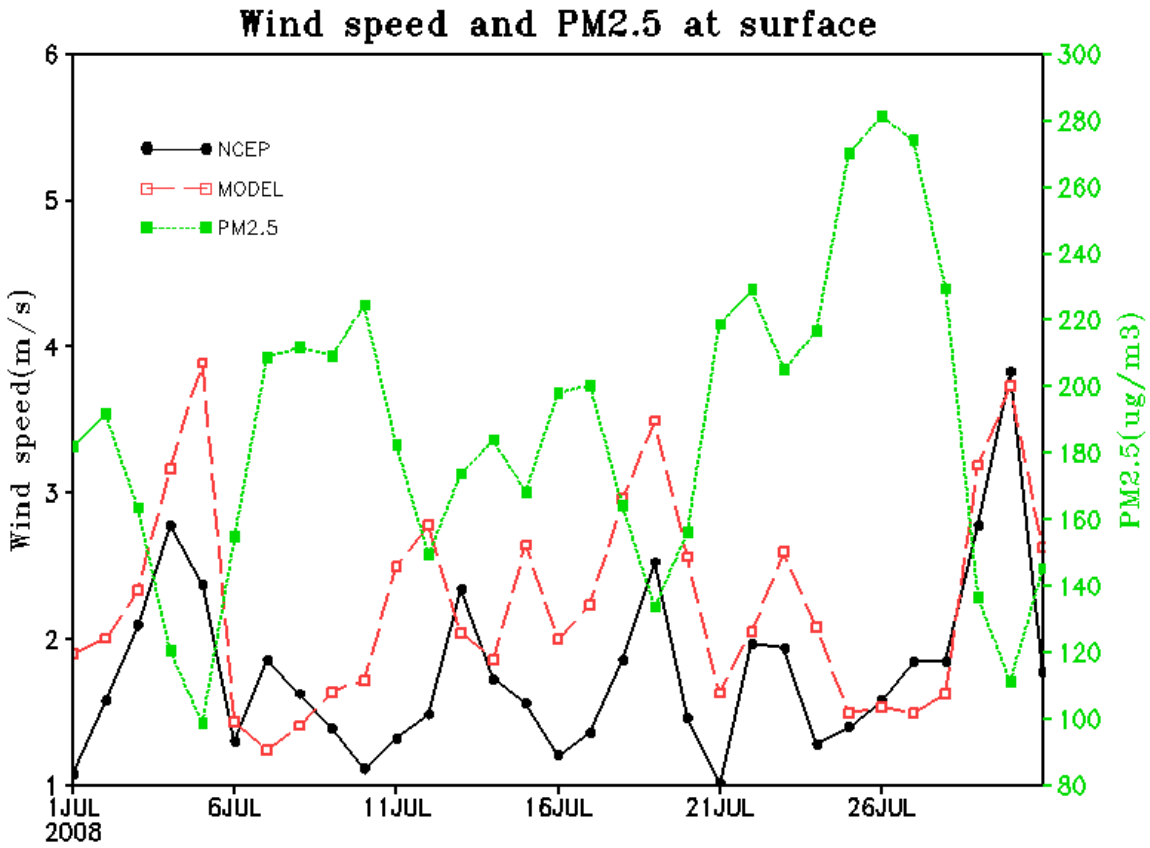

998 Fig. 7 Mean surface $PM_{2.5}$ (μg m^{-3}, contour) and f_{ktm} (m^2 s^{-1}, shaded) for 7–11
999 July, 2008 (top) and the daily changes of the 3JNS mean $PM_{2.5}$ and f_{ktm} for
1000 1–31 July, 2008 (bottom).

1001

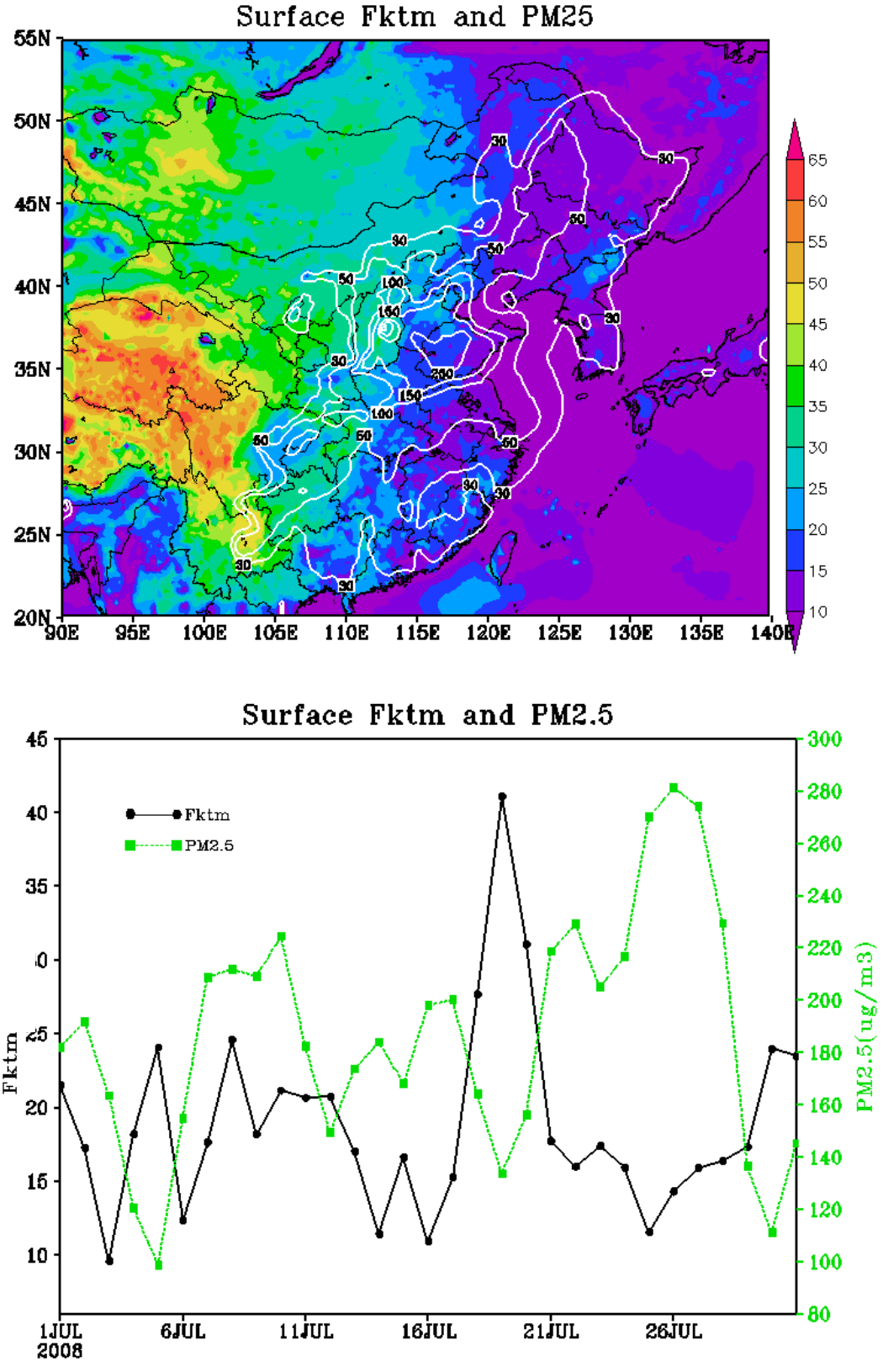

Fig. 8 The mean surface $PM_{2.5}$ (μg m^{-3}, contours) and PBL height (m, shaded) for 7–11 July, 2008 (top), and daily changes of the 3JNS mean surface $PM_{2.5}$ and PBL height (bottom).

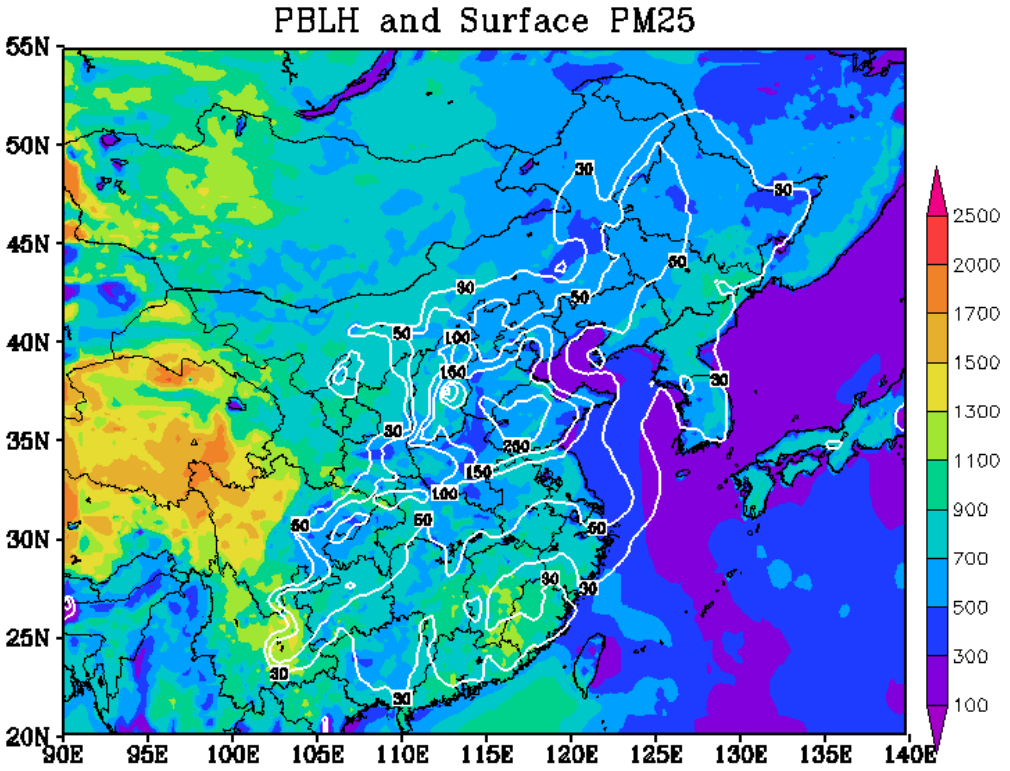

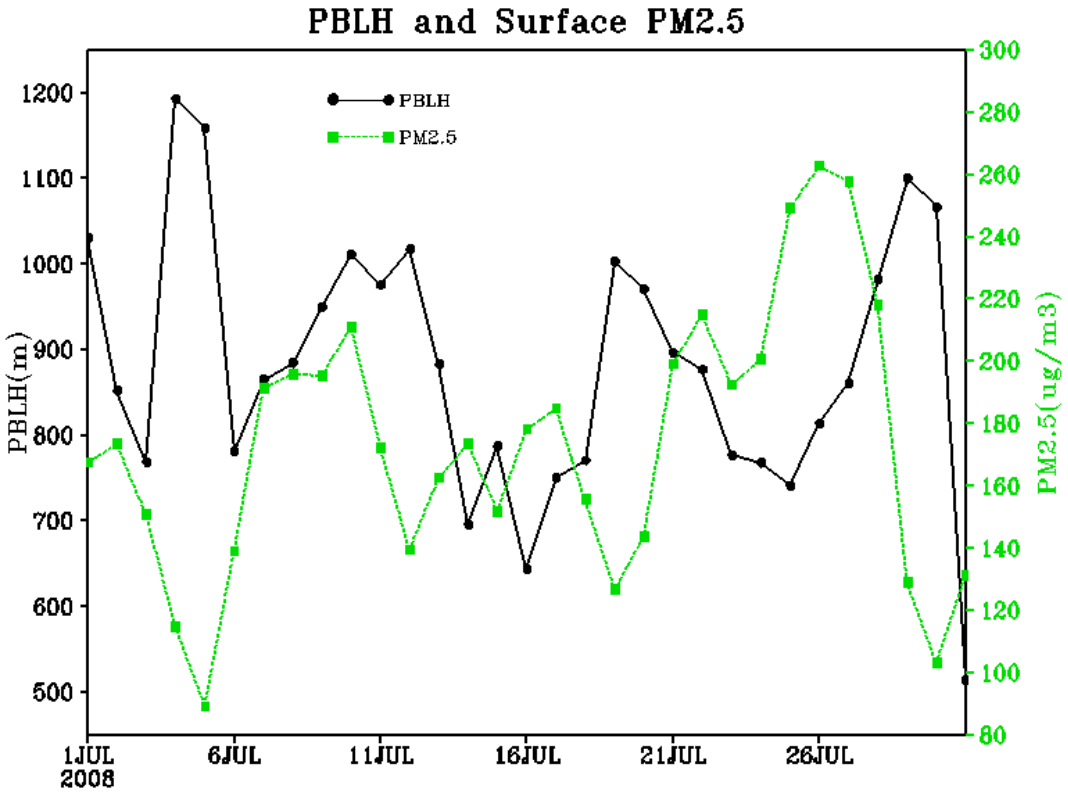

Fig. 9 Air pressure patterns (hPa, shaded), wind vectors at the surface (m s^{-1}, bottom), geopotential height (gph, shaded), wind vector at 950 hPa (middle) and 850 hPa (top) on 10 July (left) and 12 July, 2008 (right).